

See discussions, stats, and author profiles for this publication at: <https://www.researchgate.net/publication/235956812>

# Global rate coefficients for ionization and recombination of carbon, nitrogen, oxygen and argon

Article in *Physics of Plasmas* · July 2012

DOI: 10.1063/1.4737147

CITATIONS

32

READS

1,303

4 authors, including:



[Julien Annaloro](#)

Centre National d'Etudes Spatiales

42 PUBLICATIONS 125 CITATIONS

[SEE PROFILE](#)



[Vincent Morel](#)

Université de Rouen

31 PUBLICATIONS 164 CITATIONS

[SEE PROFILE](#)



[Pierre Omaly](#)

Centre National d'Etudes Spatiales

39 PUBLICATIONS 116 CITATIONS

[SEE PROFILE](#)

## Global rate coefficients for ionization and recombination of carbon, nitrogen, oxygen, and argon

Julien Annaloro, Vincent Morel, Arnaud Bultel, and Pierre Omaly

Citation: [Phys. Plasmas](#) **19**, 073515 (2012); doi: 10.1063/1.4737147

View online: <http://dx.doi.org/10.1063/1.4737147>

View Table of Contents: <http://pop.aip.org/resource/1/PHPAEN/v19/i7>

Published by the [American Institute of Physics](#).

---

### Related Articles

Collisionless kinetic regimes for quasi-stationary axisymmetric accretion disc plasmas

[Phys. Plasmas](#) **19**, 082905 (2012)

Physical conditions for fast reconnection evolution in space plasmas

[Phys. Plasmas](#) **19**, 072315 (2012)

Electron energization during magnetic island coalescence

[Phys. Plasmas](#) **19**, 072120 (2012)

On the relevance of magnetohydrodynamic pumping in solar coronal loop simulation experiments

[Phys. Plasmas](#) **19**, 072513 (2012)

Electronic excitation and isentropic coefficients of high temperature planetary atmosphere plasmas

[Phys. Plasmas](#) **19**, 072115 (2012)

---

### Additional information on Phys. Plasmas

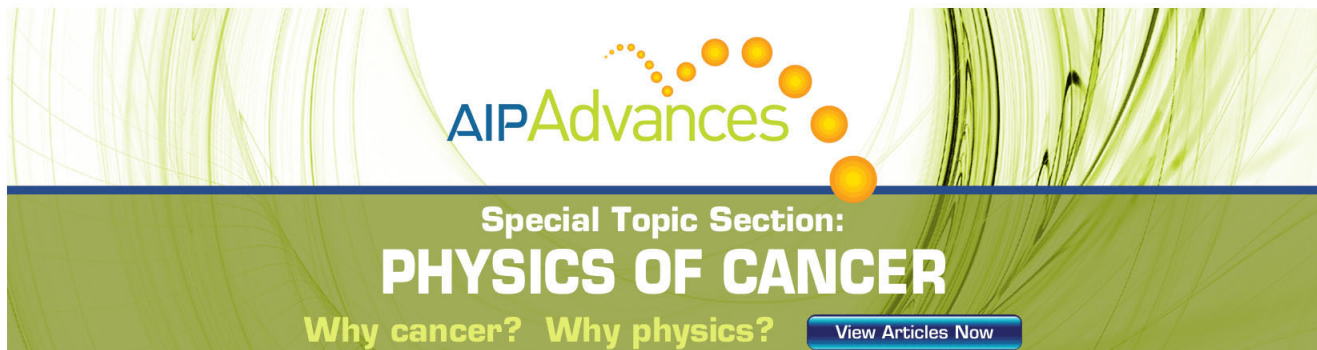
Journal Homepage: <http://pop.aip.org/>

Journal Information: [http://pop.aip.org/about/about\\_the\\_journal](http://pop.aip.org/about/about_the_journal)

Top downloads: [http://pop.aip.org/features/most\\_downloaded](http://pop.aip.org/features/most_downloaded)

Information for Authors: <http://pop.aip.org/authors>

## ADVERTISEMENT



**AIPAdvances**

Special Topic Section:  
**PHYSICS OF CANCER**

Why cancer? Why physics? [View Articles Now](#)

# Global rate coefficients for ionization and recombination of carbon, nitrogen, oxygen, and argon

Julien Annaloro,<sup>1,a)</sup> Vincent Morel,<sup>1,b)</sup> Arnaud Bultel,<sup>1,c)</sup> and Pierre Omary<sup>2,d)</sup>

<sup>1</sup>CORIA, UMR CNRS 6614, Université de Rouen, BP 12, Avenue de l'Université, 76801 Saint-Etienne du Rouvray Cedex, France

<sup>2</sup>CNES, 18 Avenue Edouard Belin, 31401 Toulouse Cedex 9, France

(Received 14 March 2012; accepted 17 June 2012; published online 23 July 2012)

The flow field modeling of planetary entry plasmas, laser-induced plasmas, inductively coupled plasmas, arcjets, etc., requires to use Navier-Stokes codes. The kinetic mechanisms implemented in these codes involve global (effective) rate coefficients. These rate coefficients result from the excited states coupling during a quasi-steady state. In order to obtain these global rate coefficients over a wide electron temperature ( $T_e$ ) range for ionization and recombination of carbon, nitrogen, oxygen, and argon, the behavior of their excited states is investigated using a zero-dimensional (time-dependent) code. The population number densities of these electronic states are considered as independent species. Their relaxation is studied within the range  $3000 \text{ K} \leq T_e \leq 20\,000 \text{ K}$  and leads to the determination of the ionization ( $k_i$ ) and recombination ( $k_r$ ) global rate coefficients. Comparisons with existing data are performed. Finally, the ratio  $k_i/k_r$  is compared with the Saha equilibrium constant. This ratio increases more rapidly than the equilibrium constant for  $T_e > 15\,000 \text{ K}$ . © 2012 American Institute of Physics. [<http://dx.doi.org/10.1063/1.4737147>]

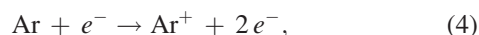
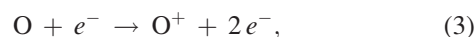
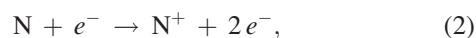
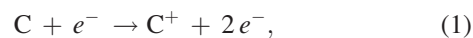
## I. INTRODUCTION

The most relevant way to model plasmas in local thermodynamic nonequilibrium is to work directly with the Boltzmann equation. Unfortunately, this equation is of the integro-differential type and cannot be treated easily.<sup>1</sup> Nevertheless, this treatment is sometimes required. For instance, when the electric field is strong,<sup>2</sup> the Boltzmann equation has to be solved. The departure from equilibrium of the electron energy distribution function (EEDF) is then strong and the resolution of the Boltzmann equation leads to the EEDF determination. Elementary chemical processes rate coefficients can be derived from integration of cross sections over the EEDF.

In many situations, plasmas depart less strongly from equilibrium. The translation mode can be balanced independently for each type of particles. The EEDF and the heavy particles energy distribution function (HEDF) are Maxwellian with different kinetic temperatures. The plasma is then in thermal nonequilibrium. It can be studied with more usual balance equations in the framework of computational fluid dynamics (CFD) if continuum hypothesis is valid. This treatment is relevant when the mean free path  $\lambda$  of electrons or heavy particles is weak enough with respect to the characteristic size  $\delta$  of the studied plasma. Dimensionless Knudsen number  $Kn = \lambda/\delta$  has to be largely smaller than unity. In addition, electric and/or magnetic influence due to external sources has to be moderate. The plasma can then be modeled by using Navier-Stokes (NS) equations coupled with simplified Maxwell equations. From the chemical point of view, elementary process rate coefficients can be calculated using Maxwellian distributions.

Since their cross sections are lower than elastic collision cross section, their characteristic time scale is longer and the plasma can be in chemical nonequilibrium. As a result, modeling a plasma in thermochemical nonequilibrium requires to solve not only the hydrodynamics problem but also the electromagnetic and chemical problems.

The modeling effort required to solve the resulting partial differential equations is significant. This resolution is time-consuming even using highly efficient computational means.<sup>3</sup> In this context, it was not possible so far to solve exactly the general problem considering a detailed chemistry, i.e., including explicitly the species excited states as independent variables. Nevertheless, some exceptions exist when the metastable states play a crucial role.<sup>4–7</sup> Except for these specific cases, the chemistry is treated from the species point of view. In other words, the excited states of each species are lumped together and the balance equations treat these species as a whole. Despite this simplification, plasma flows modeling reproduces experimental results with a satisfactory agreement. Indeed, this approach has been successfully applied to reactive flow control,<sup>8</sup> laser-induced plasmas,<sup>9–11</sup> inductively coupled plasmas,<sup>12–16</sup> arcjets,<sup>17–20</sup> plasma reactors,<sup>21–23</sup> pulsed arcs,<sup>24</sup> direct current and transient plasmas,<sup>25–27</sup> plasma-surface boundary layers,<sup>28,29</sup> cutting torches,<sup>30</sup> and magnetically controlled plasma flows.<sup>31</sup> A thorough examination of the used kinetic models reveals that the following processes are systematically taken into account:



<sup>a)</sup>Electronic mail: Julien.Annaloro@coria.fr.

<sup>b)</sup>Electronic mail: Vincent.Morel@coria.fr.

<sup>c)</sup>Electronic mail: Arnaud.Bultel@coria.fr. URL: <http://www.coria.fr/spip.php?auteur9>.

<sup>d)</sup>Electronic mail: Pierre.Omary@cnes.fr.

and their backward processes as well, when the studied plasmas involve carbon, nitrogen, oxygen, or argon. Their rate coefficients are known with a large uncertainty.<sup>32</sup> As a result, the determination of the rate coefficients is required using alternative strategy. Using updated values for modeling the different plasmas reviewed above, the modeling results may be closer to the experiments.

There is another important topic in which these processes play a significant role. Entering the atmosphere of a planet such as Earth or Mars, or a satellite such as Titan, a hypersonic body undergoes a strong heating due to the compression of the incident gas flow. Despite the low pressure of upper layers of atmosphere at which entry occurs, the compression is strong enough to reduce the mean free path considerably. The Knudsen number is then largely smaller than unity and the flow forms a shock layer around the body where the continuum assumption is valid. The modeling of the shock layer has been treated so far by considering the continuum approaches in thermochemical nonequilibrium. Electrons and heavy particles are considered as independent species with their own kinetic temperature. The entry parameters (type of atmosphere, velocity, altitude) depend strongly on the situation. The most studied case concerns Earth's reentry. For the Apollo capsule with velocity of  $11 \text{ km s}^{-1}$  at 75 km, the thickness of the shock layer is 5 cm. The maximum temperature is found just behind the shock front (5 cm from the body's surface) and corresponds to 30 000 K. At 2.5 cm, the temperature equals 10 000 K and the body's surface is at 2000 K typically. The pressure inside the shock layer is almost uniform at 5000 Pa. In these typical conditions, the flow can be modeled using NS equations.<sup>33–43</sup>

Generally speaking, in many NS approaches, the chemistry is often modeled by considering only the different species where excited and ground states are lumped together in the same description. These approaches are developed also for the modeling of flows in shock tubes,<sup>44–47</sup> high-enthalpy wind tunnels,<sup>48</sup> and nozzles<sup>43,49</sup> used as ground test facilities. However, recent developments tend to separate the excited states having slow relaxation such as vibrational states for molecules or metastable states for atoms. For example, the work of Capitelli *et al.* is clearly aiming at overcoming the classical treatment of the entry plasmas by considering state-to-state approaches and couplings with Boltzmann equation.<sup>50,51</sup> Unfortunately, they require a huge amount of elementary data which are not available for any situation. Moreover, they lead to prohibitive time calculations. The approach in terms of species is therefore widely used. State of the art CFD methods are based on shock capturing and shock fitting methodologies<sup>52</sup> where NS equations are used and species are considered as a whole. They can be applied to complete 2D flows such as the one developed around blunt bodies. In addition, they are very robust to capture complicated phenomena such as shock-shock interaction and multiple shocks in the flow field. Therefore, the usual approach based on Navier-Stokes equations and species description is in continuous improvement. The proof is the significant number of CFD codes available to calculate this type of reactive flows. The most known codes are the CelHyO,<sup>53</sup> COOLFluid,<sup>54</sup> DPLR,<sup>55</sup> LAURA,<sup>56</sup> LORE,<sup>57</sup> NERAT,<sup>58</sup> TINA,<sup>59</sup> URANUS,<sup>60</sup> US3D,<sup>61</sup> and WIND<sup>62</sup> codes.

The kinetic mechanisms used so far in these CFD codes involve the processes (1)–(4) for Earth, Mars, and Titan entries. Other ionization phenomena are also involved in these kinetic mechanisms such as charge exchange and molecular contributions. The rate coefficient of (1)–(4) is derived from the recombination rate coefficient determined experimentally and using the equilibrium constant. In addition, the rate coefficient is obtained by this way over a narrow range of electron temperature and is therefore extrapolated.<sup>32,46,47</sup> The rate reliability is therefore questionable for entry CFD simulations. We have already mentioned above the uncertainty of these rates for other plasmas where (1)–(4) can play a role. Their new determination would be particularly valuable.

The present paper deals with this determination from a theoretical point of view, and with the comparison with existing data. Only the processes (1)–(4) are studied. As a result, the real ionization or recombination of entry plasmas is not directly modeled hereafter since charge exchange and molecular contributions are ignored. The mechanisms (1)–(4) are global because they concern species, including all excited states.<sup>63</sup> Each mechanism is characterized by a global rate coefficient. Each global rate coefficient strongly depends on the behavior of the excited states. Among the works devoted to the behavior of the excited states during an ionization or a recombination phase, we can cite the ones due to Kunc and Soon<sup>64,65</sup> and Bourdon *et al.*<sup>66,67</sup> for nitrogen and oxygen, Sawada and Fujimoto for hydrogen,<sup>68</sup> and Bultel *et al.*<sup>69</sup> for argon. All these works were essentially focused (a) on the influence of radiation on the nonequilibrium, (b) on the conditions of observation of the quasi-steady state (QSS), and (c) on the calculation of ionization and recombination rate coefficients on moderate electron temperature ( $T_e$ ) ranges. As far as we know, no work has been devoted so far (1) to the nonequilibrium itself, (2) to the influence of the cross sections coupling the excited states on the nonequilibrium during the QSS and on the derived rate coefficients, and (3) to the influence of the energy diagram. In this paper, we propose therefore to focus our attention on the previous points by elaborating a time-dependent 0D collisional model based on a state-to-state description of carbon, nitrogen, oxygen, and argon in the purpose of calculating their global rate coefficient of ionization and recombination over a wide electron temperature range.

The paper presents first the model used and the cross sections adopted to describe the elementary processes between excited states. The concept of global rate coefficient is introduced and discussed. The mechanism of the ionization of oxygen is then analyzed and the procedure of identification of the global ionization rate coefficient is explained. The influence of pressure and temperature is discussed. The ionization or the recombination resulting from a stepwise mechanism, the influence of the distribution of the excited states, is also discussed. Although the elementary rate coefficients are driven by equilibrium constants, it is not necessary the case for global rates. We illustrate this peculiarity at high temperature. Finally, the global rate coefficients are interpolated under modified Arrhenius laws relevant for future implementation in CFD calculations, and they are discussed through a literature survey based on the most used data.

## II. MODEL

### A. Energy diagram

The energy diagrams of carbon, nitrogen, oxygen, and argon used in the present study are derived from the NIST database.<sup>70</sup> Table I summarizes their main characteristics. Generally speaking, density effects can be observed on the ionization potential by Debye shielding,<sup>71</sup> on energy levels,<sup>72</sup> and on elementary cross sections by dynamical screening.<sup>73</sup> With  $n_e < 10^{21} \text{ m}^{-3}$ , these effects are totally negligible. The plasma studied is, therefore, totally ideal. In the following, electron density does not exceed this limit value.

From the ionic point of view, only the ten first excited states are retained. All possible transitions between states until a dozen of eV above the ground state can then be taken into account. This is compatible with the values considered for the electron temperature  $T_e$ .

### B. Elementary processes, cross sections, and rate coefficients

Electron-induced elementary processes (excitation/deexcitation and ionization/recombination) between previous ground and excited states induce the plasma ionization or recombination. The cross section of each elementary process has to be calculated. In the past, different approaches have been developed in order to calculate them. In particular, classical approaches due to Gryzinski<sup>74</sup> and Kingston<sup>75</sup> have been developed with a limited success owing to the quantum feature of the interaction between the incoming electron and the atomic electrons at low energy. Therefore, quantum approaches have been developed particularly in the framework of the approximations of Born for atoms, and of Coulomb-Born for ions. The models due to van Regemorter<sup>76</sup> and to Vainshtein<sup>77</sup> are well known. The Born approximation is still used.<sup>78</sup> For large relative energy between electron and target, the Bethe theory has been elaborated and modified<sup>79</sup> or combined with binary-encounter-dipole model.<sup>80</sup> Cross sections in distorted-wave approximation have also been calculated in the frame of Born approximation.<sup>81,82</sup> More sophisticated methods exist. R-matrix approaches,<sup>83,84</sup> close coupling,<sup>85</sup> convergent close-coupling,<sup>86</sup> or exterior complex scaling<sup>87</sup> generally

give very good results. Unfortunately, they require intensive calculations and cannot be used for any chemical element for any kind of collision. The number of published quantum calculations is moreover too weak in comparison with the total number of transitions required for state-to-state calculations. Over the last two decades, the integrated package HULLAC has been elaborated.<sup>88</sup> This code, based on relativistic quantum mechanical calculations including configuration interaction, calculates the structure of atoms or ions, collision cross sections, radiative decay rates, autoionization, and photoionization cross sections. Collisional cross sections are calculated in the distorted wave approximation. The number of configurations and transitions required for state-to-state calculations remains very important today and prevents at the moment the use of HULLAC for the present application.

The limitations discussed above have in part motivated empirical, semi-empirical, or scaling approaches capable of sufficiently accurate prediction for any transition. The most known are due to Drawin,<sup>89</sup> Lotz,<sup>90</sup> and Vriens and Smeets.<sup>91</sup> The Lotz approach has been recently updated by Bernshtam *et al.*<sup>92</sup> Scaling approaches can be combined with quantum calculations<sup>93</sup> to obtain cross sections reliable to  $\pm 20\%$ . The cross sections proposed by Drawin present some advantages with respect to other data. Any kind of transitions (allowed transitions, spin forbidden, and parity forbidden transitions, ionization) can be considered. The cross sections are self-consistent. Their use avoids strong changes in elementary rate coefficients resulting from the implementation of different data sets and the use of unphysically correction factors.<sup>66</sup> Moreover, the Drawin's cross sections have shown their reliability in plasma physics. They have been used successfully to derive the global three-body recombination rate coefficient of  $\text{Ar}^+$  with electrons<sup>69</sup> or to model the state-to-state chemistry behind strong shock waves.<sup>94–96</sup> They have been used also in the development of collisional-radiative models for a wide range of species<sup>97–101</sup> for different applications like laser-induced plasmas,<sup>102,103</sup> plasma discharges,<sup>104</sup> and Hall thruster plasmas.<sup>105</sup> The Drawin's cross sections were therefore used in our study.

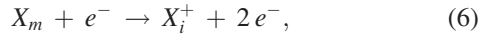
In the present work, we do not develop a modeling of one of the plasmas discussed above. We focus our attention on the electron-induced chemistry only. We consider a

TABLE I. Main characteristics of the energy diagram of carbon, nitrogen, oxygen, and argon used in this study. Energy is given in eV.

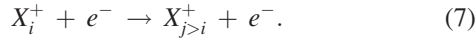
	C	N	O	Ar
Ground state	$2p^2 \ ^3P_0$	$2p^3 \ ^4S_{3/2}^o$	$2p^4 \ ^3P_2$	$3p^6 \ ^1S_0$
Metastable	$2p^2 \ ^3P_1$ (0.00203)	$2p^3 \ ^2D_{5/2}^o$ (2.38353)	$2p^4 \ ^3P_1$ (0.01962)	$3p^5 \ 4s \ ^2[3/2]_2^o$ (11.54835)
States (energy)	$2p^2 \ ^3P_2$ (0.00538)	$2p^3 \ ^2D_{3/2}^o$ (2.38461)	$2p^4 \ ^3P_0$ (0.02814)	$3p^5 \ 4s \ ^2[1/2]_0^o$ (11.72316)
	$2p^2 \ ^1D_2$ (1.26373)	$2p^3 \ ^2P_{1/2}^o$ (3.57557)	$2p^4 \ ^1D_2$ (1.96736)	
	$2p^2 \ ^1S_0$ (2.68401)	$2p^3 \ ^2P_{3/2}^o$ (3.57562)	$2p^4 \ ^1S_0$ (4.18975)	
	$2p^3 \ ^5S_2^o$ (4.18263)			
First radiative state	$2p \ 3s \ ^3P_0^o$ (7.48039)	$2p^2 \ 3s \ ^4P_{1/2}$ (10.32591)	$2p^3 \ 3s \ ^5S_2^o$ (9.14609)	$3p^5 \ 4s \ ^2[3/2]_1^o$ (11.62359)
First ionization limit $E_{ioni}$	11.26030	14.53413	13.61805	15.75961
Total number of atomic	265	251	127	379
Levels				
Total number of ionic levels	8	9	8	7



mixture of electrons, excited ions, and atoms of the same type in a uniform time-dependent closed volume  $V$  in order to study the collisional ionization or recombination of this mixture resulting from the elementary processes. Let us write  $X_m$  an atom in its excited state  $m$  and  $X_i^+$  an ion in its excited state  $i$ . Under electron impact,  $X_m$  can be excited or ionized by the elementary processes



and  $X_i^+$  can be excited according to the elementary process



By virtue of the selection rules for the dipolar transitions, the process (5) is characterized by different cross sections  $\sigma$ . Using the Drawin's cross sections, the calculation of the elementary rate coefficient under Maxwell-Boltzmann equilibrium for the kinetic energy  $\epsilon$  for the electrons is analytical. The rate coefficient is expressed as

$$k_{m \rightarrow n} = \bar{v}_e \int_a^{+\infty} y e^{-y} \sigma(y) dy, \quad (8)$$

where  $\bar{v}_e = \sqrt{\frac{8k_B T_e}{\pi m_e}}$  is the thermal electron mean velocity and  $y$  is the non-dimensional energy ratio  $\frac{\epsilon}{k_B T_e}$  the minimal value of which is  $a$ . After some algebra,<sup>103,106</sup> this expression leads to the following rate coefficients:

$$k_{m \rightarrow n}^A = \bar{v}_e 4\pi a_0^2 a^2 \alpha^A \left( \frac{E_{ion}^H}{E_n - E_m} \right)^2 I_2(a, \beta^A), \quad (9)$$

$$k_{m \rightarrow n}^P = \bar{v}_e 4\pi a_0^2 a^2 \alpha^P I_1(a), \quad (10)$$

$$k_{m \rightarrow n}^S = \bar{v}_e 4\pi a_0^2 a^2 \alpha^S I_3(a), \quad (11)$$

$$k_{m \rightarrow i}^+ = \bar{v}_e 4\pi a_0^2 a^2 \alpha^+ \left( \frac{E_{ion}^H}{E_i - E_m} \right)^2 I_2(a, \beta^+). \quad (12)$$

Respectively, these rate coefficients refer to allowed, parity forbidden, spin forbidden transitions, and ionization. They depend on the Boltzmann constant  $k_B$ , the electron mass  $m_e$ , the first Bohr radius  $a_0$ , and the ionization energy of hydrogen atom  $E_{ion}^H$ .  $E_m$ ,  $E_n$ , and  $E_i$  are the energy of the states  $m$ ,  $n$ , and  $i$ , respectively. The functions  $I_1(a)$ ,  $I_2(a, \beta^{A,+})$ , and  $I_3(a)$  are defined by

$$I_1(a) = \frac{e^{-a}}{a} - \mathcal{E}_1(a), \quad (13)$$

$$I_2(a, \beta^{A,+}) = I_1(a) \ln \left( \frac{5}{4} \beta^{A,+} \right) + \frac{\mathcal{E}_1(a)}{a} - G_2(a), \quad (14)$$

$$I_3(a) = \mathcal{E}_2(a) - \mathcal{E}_4(a), \quad (15)$$

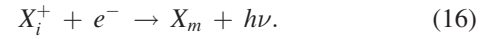
with  $\mathcal{E}_p(a)$  the exponential integral of the order  $p$  and  $G_2(a)$  the generalized exponential integral of the second order.<sup>107</sup>

In Eqs. (9) to (12), the parameters  $\alpha^A$ ,  $\alpha^P$ ,  $\alpha^S$ ,  $\alpha^+$ , and  $\beta^{A,+}$  are chosen as mean values resulting from the

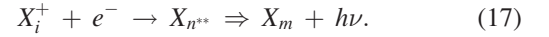
comparisons with available experimental cross sections ( $\alpha^A = 1$ ,  $\alpha^P = 0.05$ ,  $\alpha^S = 0.1$ ,  $\alpha^+ = 0.67$ ,  $\beta^{A,+} = 1$ ).

The backward processes of (5)–(7) are taken into account in order to describe equilibrium, steady state, or recombination of the mixture (see Sec. II C).

From the elementary point of view, other types of processes can occur. The first one involves radiation during radiative recombination



The second recombination process involves autoionizing levels  $n^{**}$  of the atoms through the dielectronic recombination



These processes are disregarded in the present study since our approach has in part as main objective the estimate of global rate coefficients to be implemented in Navier-Stokes codes. These rates are consequently purely collisional and exclude the radiative phenomena. Moreover, the rate coefficients of (16) and (17) have a significant value only for transitions to low excited states and the ground state.<sup>108,109</sup> Owing to the population density of these states, the radiation is anyway completely self-absorbed.

### C. Backward processes and elementary balance equations

The rate coefficients of the backward processes of (5)–(7) are calculated using the elementary equilibrium constants, i.e., the Boltzmann  $K_{n,m}^B$  and Saha  $K_{i,m}^S$  equilibrium laws, respectively. From the definition of the reaction rate,<sup>110</sup> we have

$$\begin{aligned} \frac{1}{V} \left( \frac{dN_{X_m}}{dt} \right)_{m \leftrightarrow n} &= -\frac{1}{V} \left( \frac{dN_{X_n}}{dt} \right)_{m \leftrightarrow n} \\ &= -k_{m \rightarrow n} \left( 1 - \frac{[X_n]}{[X_m] K_{n,m}^B} \right) [X_m] n_e \end{aligned} \quad (18)$$

for the excitation/deexcitation between the two levels  $m$  and  $n$ . For the ionization/recombination between the two levels  $m$  and  $i$ , we have

$$\begin{aligned} \frac{1}{V} \left( \frac{dN_{X_m}}{dt} \right)_{m \leftrightarrow i} &= -\frac{1}{V} \left( \frac{dN_{X_i^+}}{dt} \right)_{m \leftrightarrow i} \\ &= -k_{m \rightarrow i}^+ \left( 1 - \frac{[X_i^+] n_e}{[X_m] K_{i,m}^S} \right) [X_m] n_e. \end{aligned} \quad (19)$$

In both cases, the mixture is assumed to be uniform. In Eqs. (18) and (19),  $N_{X_m}$  is the number of atoms on the excited state  $m$  in the closed volume  $V$  (as a result,  $[X_m] = N_{X_m}/V$  is their population density). This volume is time-dependent for reasons given in Sec. II D.

### D. Global rate coefficients

Equations (18) and (19) written systematically for all combinations lead to

$$\begin{aligned} \frac{1}{V} \frac{dN_{X_m}}{dt} = & - \sum_{n>m} k_{m \rightarrow n} \left( 1 - \frac{[X_n]}{[X_m] K_{n,m}^B} \right) [X_m] n_e \\ & + \sum_{n<m} k_{n \rightarrow m} \left( 1 - \frac{[X_m]}{[X_n] K_{m,n}^B} \right) [X_n] n_e \\ & - \sum_i k_{m \rightarrow i}^+ \left( 1 - \frac{[X_i^+] n_e}{[X_m] K_{i,m}^S} \right) [X_m] n_e \end{aligned} \quad (20)$$

and

$$\begin{aligned} \frac{1}{V} \frac{dN_{X_i^+}}{dt} = & - \sum_{j>i} k_{i \rightarrow j} \left( 1 - \frac{[X_j^+]}{[X_i^+] K_{j,i}^B} \right) [X_i^+] n_e \\ & + \sum_{j<i} k_{j \rightarrow i} \left( 1 - \frac{[X_i^+]}{[X_j^+] K_{i,j}^B} \right) [X_j^+] n_e \\ & + \sum_m k_{m \rightarrow i}^+ \left( 1 - \frac{[X_i^+] n_e}{[X_m] K_{i,m}^S} \right) [X_m] n_e \end{aligned} \quad (21)$$

by summation.

The species variation rate is then deduced from

$$\frac{1}{V} \frac{dN_X}{dt} = \sum_m \frac{1}{V} \frac{dN_{X_m}}{dt}$$

for the neutrals and from

$$\frac{1}{V} \frac{dN_{X^+}}{dt} = \sum_i \frac{1}{V} \frac{dN_{X_i^+}}{dt} \quad (22)$$

for the ions inside  $V$ .

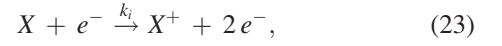
These equations allow the computation of either an ionization configuration or a recombination configuration. Once pressure  $p$  and the temperature  $T_e$  chosen, an ionization configuration is obtained if the initial electron density  $n_e(t=0)$  is lower than the electron density at equilibrium  $n_e^S$  given by

$$n_e^S = K^S \left( \sqrt{1 + \frac{p}{K^S k_B T_e}} - 1 \right),$$

where  $K^S$  is the Saha equilibrium law. A recombination configuration is obtained if  $n_e(t=0) > n_e^S$ . Electroneutrality is assumed whatever the conditions.

Thus, the mixture is assumed in ionization nonequilibrium. If  $n_e(t=0) < n_e^S$ , the ionization elementary processes are not balanced by the recombination elementary processes as illustrated by Fig. 1 for oxygen. The lack of electrons leads to the ionization of all atomic states, therefore to the decrease of their number. Then, the elementary excitation processes are not balanced by the elementary deexcitation processes. Thus, the lack of electrons leads to the ionization from the neutral (ground and excited) states to the (ground and excited) ionic states. The total number of atoms is therefore decreasing while that of the ions is increasing.

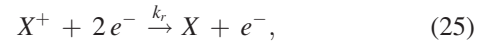
This ionization configuration can be globally represented by



where  $k_i$  is the global ionization rate.  $X$  and  $X^+$  represent the atoms and ions inside  $V$ , including all their excited states. This rate coefficient therefore includes the influence of the excited states on ionization through elementary processes. Equation (23) indicates that the ionization inside  $V$  is a second order process. The ionization can then be mathematically described by the differential equation

$$\frac{1}{V} \frac{dN_{X^+}}{dt} = \frac{1}{V} \frac{dN_e}{dt} = - \frac{1}{V} \frac{dN_X}{dt} = k_i [X] n_e. \quad (24)$$

When  $n_e(t=0) > n_e^S$ , the contrary case is observed. The excess of electrons leads to a higher rate for elementary recombination and deexcitation, then to the global recombination inside  $V$  according to



where  $k_r$  is the global recombination rate. The process is of third order and the differential equation similar to Eq. (24) is then

$$\frac{1}{V} \frac{dN_{X^+}}{dt} = \frac{1}{V} \frac{dN_e}{dt} = - \frac{1}{V} \frac{dN_X}{dt} = -k_r [X^+] n_e^2. \quad (26)$$

It is customary to express the net change rate of ions or electrons in the form<sup>32,111</sup>

$$\frac{1}{V} \frac{dN_{X^+}}{dt} = \frac{1}{V} \frac{dN_e}{dt} = - \frac{1}{V} \frac{dN_X}{dt} = k_i [X] n_e - k_r [X^+] n_e^2 \quad (27)$$

in order to describe in the same formalism either an ionization situation or a recombination situation. At equilibrium, we have  $d/dt \equiv 0$  and (27) leads to

$$\frac{k_i}{k_r} = \left( \frac{[X^+] n_e}{[X]} \right)_{eq} \equiv K^S, \quad (28)$$

if  $k_i \neq 0$  and  $k_r \neq 0$ . This equation is generally accepted even if it is an approximation.<sup>112,113</sup> However, Eq. (28) is basically incorrect. Indeed, in nonequilibrium when collisions are dominant, the excited states are overpopulated with respect to equilibrium in case of recombination or underpopulated with respect to equilibrium in case of ionization.<sup>96,114–117</sup> As a result, the ratio  $k_i/k_r$  departs from an equilibrium constant. Therefore, the consistency between (27) and equilibrium requires  $k_i = 0$  and  $k_r = 0$  at equilibrium, which means that  $k_i$  and  $k_r$  have transient values. The excited states influence prevents, therefore,  $k_i$  and  $k_r$  from being constant.

Nevertheless, given the temperature, the excited states reach a quasi-steady state during ionization or recombination. This leads to constant values for  $k_i$  or  $k_r$  during these states. The rate coefficients can then be identified for the given temperature. The Saha equilibrium constant is pressure-dependent.<sup>118</sup> In order to make comparisons between the resulting ratio  $k_i/k_r$  and  $K^S$ , therefore to test (28), we have performed our calculations also at given pressure.

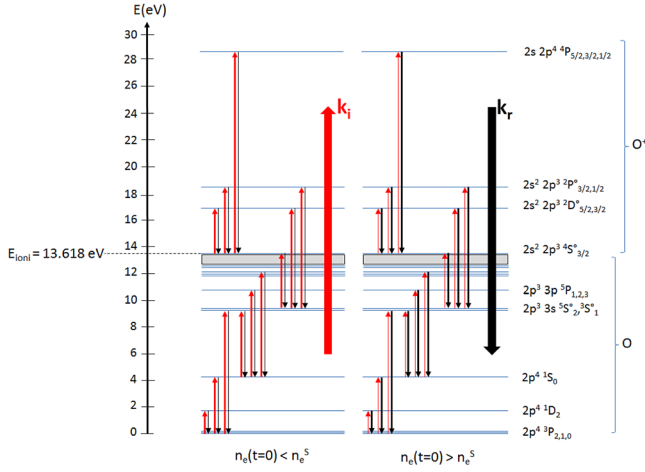


FIG. 1. Schematic view of the energy diagram of oxygen displaying the elementary couplings between all states. The Rydberg levels (close to the ionization limit) are in the gray box. Left,  $n_e(t=0) < n_e^S$ . Each level is coupled with all the others. For clarity, only a part of the possible transitions is given. Each corresponding rate is represented by an arrow in red for excitation or ionization, in black for deexcitation or recombination. The thickness of the arrows is proportional to the rate. The lack of electrons leads to the ionization from the neutral (ground and excited) states to the (ground and excited) ionic states. The total number of atoms is therefore decreasing while that of the ions is increasing. This global ionization process is then represented by  $k_i$  corresponding to the large red arrow.

Therefore, the total density is constant, which leads to the increase of  $V$  in case of ionization and to the decrease of  $V$  in case of recombination, because the total number  $N$  of particles inside  $V$  increases in case of ionization and decreases in case of recombination. Finally, coupling the previous equations with the energy balance is not required since pressure and temperature are kept constant.

### III. RESULTS AND DISCUSSION

#### A. Quasi-steady state and global rate coefficient

This section reports the results obtained at low pressure in order to show clearly the underlying dynamics. For  $p = 10^{-3}$  Pa and  $T_e = 6000$  K, Figure 2 illustrates a typical evolution of the population densities of oxygen in ionization configuration since  $n_e(t=0) < n_e^S$ . The initial level of population densities for the excited states has been chosen so that the excitation temperature defined as

$$T_{exc} = - \frac{1}{k_B \left[ \frac{d}{dE_m} \left( \ln \left[ \frac{X_m}{g_m} \right] \right) \right]_{ls}} \quad (29)$$

is equal to 6000 K. In Eq. (29),  $ls$  means that the derivative is the slope of the least square line.

Three successive phases can be observed. Their dynamics can be understood keeping in mind Fig. 1.

- **Relaxation:** From  $t = 0$  until  $t \approx \tau_{QSS} = 5 \times 10^3$  s, the excited states population densities relax owing to the initial conditions. The lack of electrons with respect to equilibrium leads to the pumping of atoms from the excited states. Their number density decreases. The depopulation propagates towards the ground state. Owing to the order

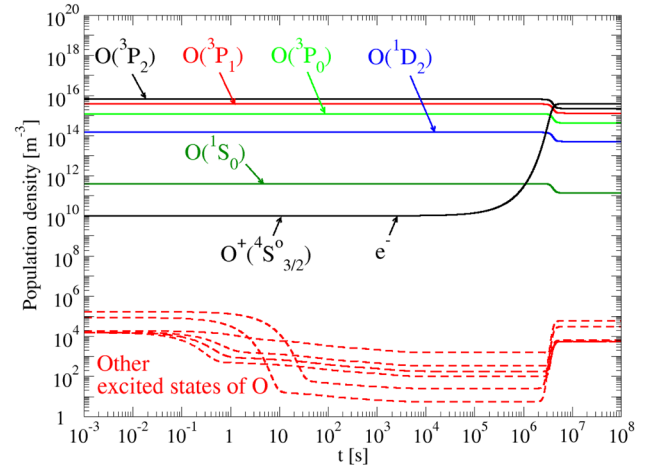


FIG. 2. Time evolution of the population density of the ground state ( $^3P_2$ ), metastable states ( $^3P_1$  to  $^1S_0$ ), and other excited states of oxygen for an ionization configuration at  $T_e = 6000$  K and  $p = 10^{-3}$  Pa. The initial excitation temperature defined as Eq. (29) is  $T_{exc} = 6000$  K and the initial electron density is  $10^{10} \text{ m}^{-3}$ .  $p$  and  $T_e$  are constant. The three successive phases are observed: (1) relaxation  $0 < t < \tau_{QSS} = 5 \times 10^3$  s, (2) quasi-steady state  $\tau_{QSS} = 5 \times 10^3 \text{ s} < t < 2 \times 10^6$  s, (3) final equilibrium state  $t > 2 \times 10^6$  s.

of magnitude for these densities, the influence of this global depopulation on metastable states  $^3P_1$  to  $^1S_0$  is negligible.

- **Quasi-steady state:** Between  $t \approx \tau_{QSS} = 5 \times 10^3$  s and  $t \approx 2 \times 10^6$  s, the excited states reach a quasi-steady value corresponding to lower densities with respect to equilibrium. The depopulation reached the ground state. During this phase, the  $[X_m]$  density changes respect the condition

$$\left| \frac{t}{[X_m]} \frac{d[X_m]}{dt} \right| < 0.05.$$

The underpopulation of the excited states is maintained because the electron density is less than  $n_e^S$ . During this phase, the electron density (equal to the ionic density owing to the electroneutrality) increases. The changes of the metastable and ground states number densities are negligible as long as electron density is too small.

- **Final equilibrium state:** When the electron density reaches a value close to  $n_e^S$ , the recombination elementary phenomena begin to play an important role. This leads to an increase of the atomic population densities close to the ionization limit. In these conditions, the level of  $n_e$  is also sufficiently high to induce the decrease of the ground state density, the global density remaining constant. The equilibrium situation is quickly reached by this way, which is easily seen on Fig. 2. For  $t > 6 \times 10^6$  s, the mixture does not evolve anymore and  $n_e = n_e^S$ .

In order to estimate the relevant conditions required to determine  $k_i$ , we follow in time parameter  $k_i^*$  defined as

$$k_i^* = - \frac{1}{[X] n_e} \left( \frac{d[X]}{dt} + \frac{[X]}{V} \frac{dV}{dt} \right). \quad (30)$$

Introducing the density in the left-hand side of Eq. (24), the latter equation becomes



$$\frac{d[X]}{dt} = -k_i[X]n_e - \frac{[X]}{V} \frac{dV}{dt},$$

the form of which allows the comparison between  $k_i^*$  and  $k_i$ .

Figure 3 displays the evolution of  $k_i^*$  in the conditions of Fig. 2. One can observe also for  $k_i^*$  the three phases put forward previously for the excited states population densities. In particular, we clearly see the QSS for which  $k_i^*$  is time-independent. In addition, when  $t > 3 \times 10^6$  s, the value of  $k_i^*$  collapses because equilibrium is reached. On this figure, we also show the results obtained for other initial conditions. For a very small initial electron density, or a higher initial excitation temperature, we obtain other time evolutions for the excited states population densities and for  $k_i^*$ . Although the level of population densities is different during the QSS, the value derived for  $k_i^*$  is the same as the previous one during the quasi-steady state. During the QSS,  $k_i^*$  therefore depends on  $p$  and  $T_e$  only. These conditions lead to the conclusion that  $k_i$  must be identified with  $k_i^*$  during the quasi-steady state.

It is interesting to study the evolution of  $T_{exc}$  defined by Eq. (29). Figure 4 displays this evolution in the conditions of Fig. 2. The evolution of the ionization temperature defined as

$$T_{ioni} = \frac{E_{ioni}}{k_B \ln \left[ 2 \frac{g_0^+}{g_0} \frac{[X_0]}{[X_0^+]} n_e \left( \frac{2 \pi m_e k_B T_e}{h^2} \right)^{3/2} \right]}, \quad (31)$$

where subscript 0 indicates that the quantity is related to the ground state, is also displayed. The three phases can be easily observed. In particular, we can notice the initial excitation temperature chosen at  $T_{exc} = 6000$  K. When the QSS is reached, both  $T_{exc}$  and  $T_{ioni}$  are lower than  $T_e$ .  $T_{exc}$  does not evolve during the QSS, conversely to  $T_{ioni}$ . This is due to the definition of  $T_{ioni}$  which involves both ionic and atomic densities. Conditions  $T_{exc} \neq T_e$  and  $T_{ioni} \neq T_e$  are not surprising in the present case. Indeed, Eqs. (18) and (19) indicate that

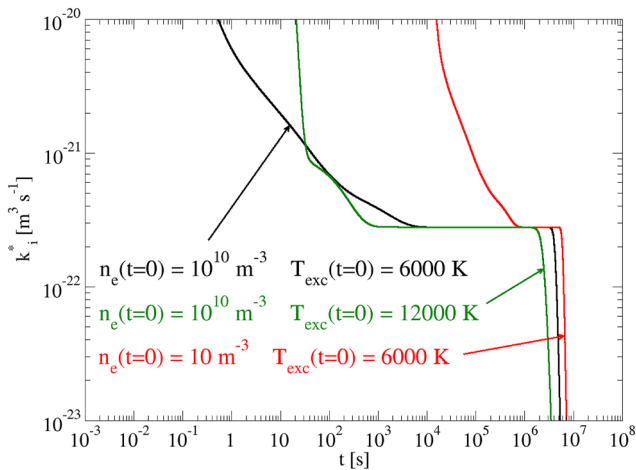


FIG. 3. Time evolution of the parameter  $k_i^*$  defined by Eq. (30) for different initial conditions at  $T_e = 6000$  K and  $p = 10^{-3}$  Pa for oxygen. The conditions ( $n_e(t=0) = 10^{10} \text{ m}^{-3}$ ,  $T_{exc}(t=0) = 6000$  K) correspond to Fig. 2. The three successive phases already seen on Fig. 2 are observed. In particular, the quasi-steady state characterized by  $\partial k_i^* / \partial t = 0$  is obvious.

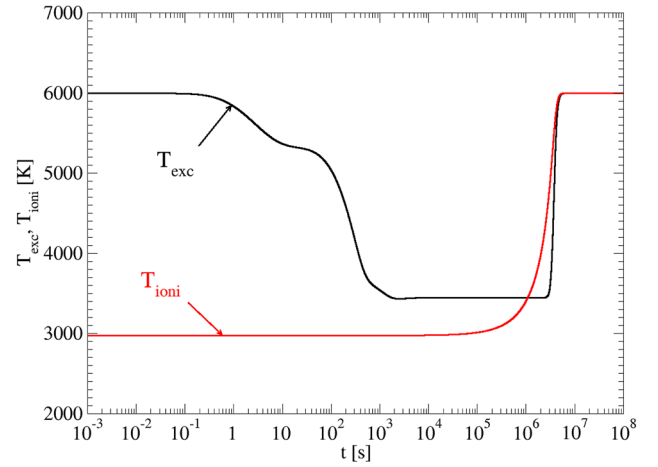


FIG. 4. Time evolution of  $T_{exc}$  and  $T_{ioni}$ , defined by Eqs. (29) and (31), respectively, for the ionization configuration of Fig. 2 ( $p = 10^{-3}$  Pa,  $T_e = 6000$  K,  $n_e(t=0) = 10^{10} \text{ m}^{-3}$ ,  $T_{exc}(t=0) = 6000$  K).

the parenthesis of their right-hand side would be equal to 0 if the equilibrium were fulfilled. However, the system evolving once again after the QSS means that this state does not correspond to equilibrium. Each forward elementary process is not therefore rigorously counterbalanced by the corresponding backward elementary process. The right-hand side of the previous equations does not equal 0. As a result,  $T_{exc}$  and  $T_{ioni}$  depart from  $T_e$ . Moreover, the electron density is smaller than the equilibrium value  $n_e^s$  during this phase. The ionization temperature is therefore less than the equilibrium value  $T_e$ . For  $t > 6 \times 10^6$  s, the equilibrium is observed with  $T_{exc} = T_{ioni} = T_e$ .

In the case of recombination configurations,  $T_{exc}$  and  $T_{ioni}$  are higher than  $T_e$  during the QSS. The values of  $k_r^*$ , defined as

$$k_r^* = - \frac{1}{[X^+] n_e^2} \left( \frac{d[X^+]}{dt} + \frac{[X^+]}{V} \frac{dV}{dt} \right), \quad (32)$$

do not depend on the initial conditions during the quasi-steady state and can be consequently identified with  $k_r$  during the QSS.

## B. Influence of the pressure

The mixture considered is an ideal gas since the independence of the energy diagram and the cross sections from density is complete. The rate coefficients have therefore to be independent from pressure  $p$ . We have verified this basic property by performing the calculations in different pressure levels. The increase of the pressure leads to an increase of the collision frequency. The characteristic time scales decrease and the time evolutions are faster. Sometimes, the reduction of the time scales is sufficiently large to prevent a correct observation of the quasi-steady state. This explains why such a weak value for  $p$  has been chosen previously in order to allow a clear view of the QSS. Nevertheless, in most cases, the quasi-steady state is obvious, as shown by Fig. 5 for oxygen. This figure displays the values of  $k_i^*$  obtained for the same temperature  $T_e = 6000$  K with different pressure

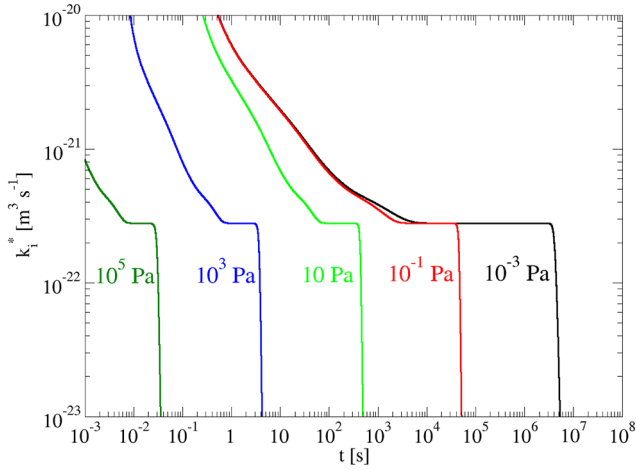


FIG. 5. Time evolution of  $k_i^*$  defined by Eq. (30) for oxygen at  $T_e = 6000$  K, for different levels of pressure between  $10^{-3}$  Pa and  $10.5$  Pa ( $n_e(t=0) = 10^{10} \text{ m}^{-3}$ ,  $T_{exc}(t=0) = 6000$  K).

values. A limit pressure of  $10^5$  Pa has been chosen, but the QSS can be observed at this temperature also for  $10^6$  Pa. We can notice the presence of a plateau, the start and duration of which increase when the pressure decreases. The corresponding value of  $k_i^*$  is the same in all cases. Since the value of  $k_i$  must depend on  $T_e$  only, the rate coefficient for ionization is therefore the one obtained during the QSS, that is during the plateau. Concerning the recombination, the situation is once again totally symmetric to the ionization. The values of  $k_r^*$  calculated with Eq. (32) present a plateau for the quasi-steady state, the value of which is only  $T_e$ -dependent. Rate coefficient  $k_r$  corresponds therefore to the value of  $k_r^*$  taken during the plateau.

### C. Influence of the temperature

Section III B has shown that  $p$  does not influence the global rate coefficients either for ionization or for recombination. The thermodynamic parameter which modifies the global rate coefficient is only temperature  $T_e$ . Almost in all cases, the determination of rate coefficient  $k_i$  or  $k_r$  by identification during the quasi-steady state with  $k_i^*$  or  $k_r^*$  is possible. This determination is performed over the range  $3000 \text{ K} \leq T_e \leq 20000 \text{ K}$ . The temperature limit of  $3000 \text{ K}$  or  $20000 \text{ K}$  results from the weak values obtained for  $k_i$  and  $k_r$  at low and high temperatures, respectively.

The previous study of the dynamics of the excited states is systematically performed for the carbon, oxygen, nitrogen, and argon atoms listed in Table I over the range  $3000 \text{ K} \leq T_e \leq 20000 \text{ K}$ . In the following, we focus our attention on the global rate coefficients  $k_i$  and  $k_r$  only.

Figure 6 illustrates the  $T_e^{-1}$  dependence of  $k_i$ . We can notice that  $k_i(\text{C}) > k_i(\text{O}) \simeq k_i(\text{N}) > k_i(\text{Ar})$ . The carbon ionization rate coefficient is systematically higher than for nitrogen, oxygen, and argon. N and O present a very similar behavior and the ionization of Ar is more difficult, whatever the value of  $T_e$ . These characteristics result mainly from the energy diagrams summarized in Table I. Indeed, the ionization limit of the different atoms is ordered, such as  $E_{ioni}(\text{C}) < E_{ioni}(\text{O}) \lesssim E_{ioni}(\text{N}) < E_{ioni}(\text{Ar})$ .

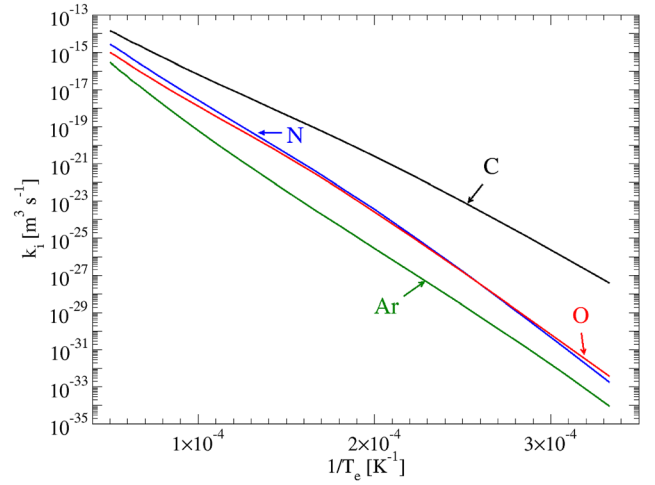


FIG. 6. Evolution of the global ionization rate coefficient  $k_i$  (identified with  $k_i^*$  following the procedure of Sec. III A) with respect to  $1/T_e$  for carbon, nitrogen, oxygen, and argon.

The curve form of Fig. 6 clearly shows that an interpolation under a modified (three factors) Arrhenius law

$$k_i = A_i T_e^{\alpha_i} e^{-\frac{T_i}{T_e}} \quad (33)$$

is convenient. Indeed, the departure from a linear shape results from the order of magnitude of  $\alpha_i$ . One can observe on Fig. 6 the weakness of this departure in every case. The corresponding values of  $A_i$ ,  $\alpha_i$ , and  $T_i$  required by Eq. (33) are given in Table II. Globally, they interpolate the rate coefficients calculated with our approach within a factor of 2 at maximum.

It is interesting to comment the values obtained for the characteristic temperature  $T_i$ . Table II also gives the values of  $E_{ioni}/k_B$ . They can be compared with  $T_i$ . For carbon, nitrogen, and oxygen, the agreement between  $T_i$  and  $E_{ioni}/k_B$  is very good. This is not surprising. Indeed, this agreement results from fundamental properties. Table I shows that the energy diagram of these atoms is relatively progressive, insofar as the energy difference between successive levels does not exceed  $6.75 \text{ eV}$  (case of nitrogen). Even for low temperatures, the excitation is relatively easy. The ionization being a process requiring a threshold in energy equal to the ionization limit, the characteristic temperature involved by the Arrhenius law is therefore this limit. A good agreement between  $E_{ioni}/k_B$  and  $T_i$  has to be therefore observed. In the case of argon, the energy diagram is less favorable to a good coupling. Indeed, the most important energy difference between successive levels exceeds  $11.5 \text{ eV}$ , which corresponds to the gap between the ground state and the first metastable state  $3p^5 4s$ . In the case of low temperatures, the process of population of the first metastable state is therefore difficult and limits the ionization. As a result, this second threshold plays a role. This effect has been already discussed by Hoffert and Lien.<sup>113</sup> Since the interpolation (33) is obtained over the range  $3000 \text{ K} \leq T_e \leq 20000 \text{ K}$ , the characteristic temperature  $T_i$  is then lower than  $E_{ioni}/k_B$ . This interpretation is emphasized by the asymptotic behavior of Eqs. (8)–(15). In case no excited state exists between the

TABLE II. Parameters of the Arrhenius interpolations (33) and (35) for  $k_i$  and  $k_r$ , given in  $\text{m}^3 \text{s}^{-1}$  and  $\text{m}^6 \text{s}^{-1}$ , respectively. The values of  $E_{\text{ioni}}/k_B$  are given for direct comparison with  $T_i$ .  $E_{\text{ioni}}/k_B$ ,  $T_i$ , and  $T_r$  are given in K.

Arrhenius interpolation Process	$k_i = A_i T_e^{\alpha_i} e^{-T_i/T_e}$				$k_r = A_r T_e^{\alpha_r} e^{-T_r/T_e}$		
	$A_i$	$\alpha_i$	$T_i$	$[E_{\text{ioni}}/k_B]$	$A_r$	$\alpha_r$	$T_r$
$\text{C} + e^- \xrightleftharpoons[k_r]{k_i} \text{C}^+ + 2e^-$	$9.72 \times 10^{-3}$	-2.074	127 510	[130 670]	$4.27 \times 10^{-29}$	-2.487	-12 260
$\text{N} + e^- \xrightleftharpoons[k_r]{k_i} \text{N}^+ + 2e^-$	32	-2.856	168 970	[168 660]	$5.17 \times 10^{-25}$	-3.476	-5460
$\text{O} + e^- \xrightleftharpoons[k_r]{k_i} \text{O}^+ + 2e^-$	$1.37 \times 10^{-2}$	-2.237	157 840	[158 030]	$2.87 \times 10^{-22}$	-4.135	1790
$\text{Ar} + e^- \xrightleftharpoons[k_r]{k_i} \text{Ar}^+ + 2e^-$	$1.23 \times 10^{-19}$	1.511	141 480	[182 880]	$9.41 \times 10^{-44}$	0.368	-45 430

atomic and ionic ground states, global ionization rate coefficient  $k_i$  is close to  $k_{m \rightarrow n}^+$  where  $m$  is the atomic ground state and  $n$  is the ionic ground state. Moreover,  $a$  equals  $\frac{E_{\text{ioni}}}{k_B T_e}$  the value of which is relatively large ( $a > 5$ ). In these conditions, we have<sup>119</sup>

$$\mathcal{E}_1(a) \cong e^{-a} \left(1 + \frac{1}{a}\right)$$

and

$$G_2(a) \cong \frac{g(a)}{a^2} e^{-a},$$

where  $g(a)$  is a Chebyshev polynomial<sup>107</sup> slowly evolving with  $a$ . The rate coefficient finally writes as

$$k_i = \bar{v}_e 4\pi a_0^2 \alpha^+ \left(\frac{E_{\text{ion}}^H}{E_{\text{ioni}}}\right)^2 \left[1 - g\left(\frac{E_{\text{ioni}}}{k_B T_e}\right)\right] e^{-\frac{E_{\text{ioni}}}{k_B T_e}}, \quad (34)$$

where we can notice the presence of  $E_{\text{ioni}}/k_B$  in the exponential term comparable to  $T_i$  in the Arrhenius interpolation (33). Thus, the existence of states corresponding to high excitation energy causes the  $T_i$  departure from  $E_{\text{ioni}}/k_B$ .

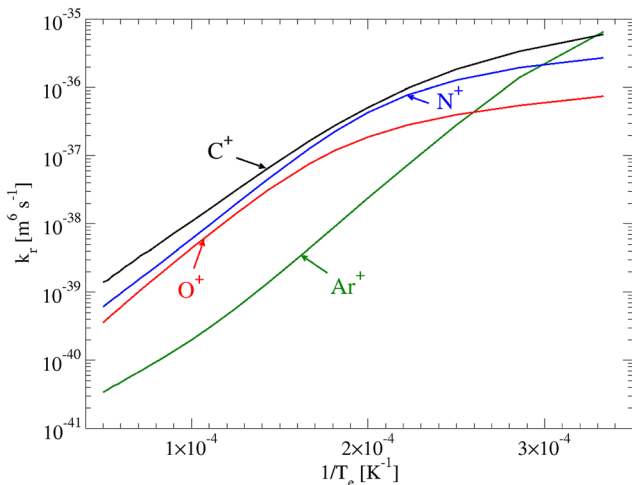


FIG. 7. Evolution of the global recombination rate coefficient  $k_r$  (identified with  $k_r^+$  following the procedure of Sec. III A) with respect to  $1/T_e$  for  $\text{C}^+$ ,  $\text{N}^+$ ,  $\text{O}^+$ , and  $\text{Ar}^+$ .

Figure 7 displays the results obtained for the recombination of ions. Table II lists the parameters  $A_r$ ,  $\alpha_r$ , and  $T_r$  allowing the best interpolation with the modified Arrhenius form

$$k_r = A_r T_e^{\alpha_r} e^{-\frac{T_r}{T_e}}. \quad (35)$$

The recombination is a process without any threshold, the electron-ion interaction potential being attractive. In these conditions, the recombination temperature  $T_r$  has to be close to 0. Once again, we can notice that this theoretical consideration is in relatively good agreement with the results obtained for carbon, nitrogen, and oxygen. However, the discrepancy is higher in the case of argon. This discrepancy is ascribed to the same reason as for ionization.

#### D. Influence of the distribution of excited states

Since argon presents a behavior different from the other species studied in this paper owing to its particular energy diagram, we focus our attention in this section to this aspect. We have calculated the global rate coefficient for ionization  $k_i$  within the same approach as the one described in Sec. III A but by treating the three following alternative energy diagrams:

- *Diagram 1.* Real levels are in part lumped together in fictitious levels, the statistical weight of which corresponds to the summation of the individual degeneracy. Within this energy diagram (due to Vlček<sup>7</sup>), the value of energy results from a mean weighted by the degeneracy of the real levels starting from an effective principal quantum number of 11. The number of states is therefore conserved.
- *Diagram 2.* The NIST energy diagram is completed with Rydberg levels assumed of the hydrogenlike type until an effective principal quantum number  $n^* \cong 700$  (the total number of levels is then 1000). The degeneracy of each Rydberg level is equal to unity.
- *Diagram 3.* Diagram 2 is assumed, but with individual degeneracies equal to  $2n^{*2}$ . The diagram fully belongs to the hydrogenlike type between the last level of the NIST database and the ionization limit.

Figure 8 illustrates the results obtained in each case, compared with the reference results of Fig. 6. We can notice that using energy *diagram 1* leads to a systematic underestimate of the ionization rate coefficient, especially important at low

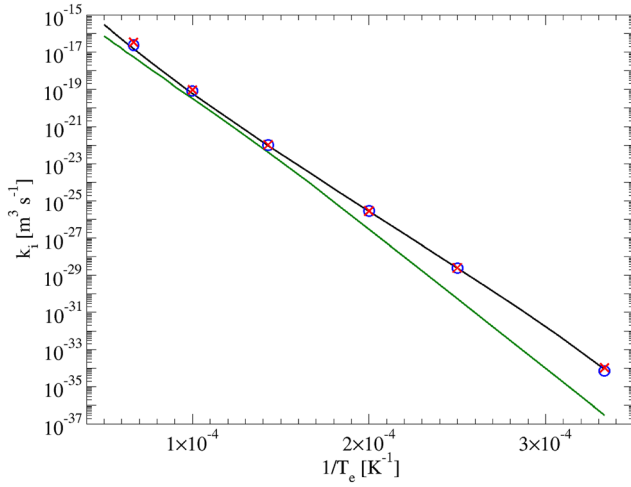


FIG. 8. Global ionization rate coefficient  $k_i$  of argon in the case of (a) the energy diagram 1 (green curve), (b) the energy diagram 2 (red crosses), and (c) the energy diagram 3 (blue circles). The reference results of Fig. 7 correspond to the black curve.

temperature. At 3000 K, the discrepancy is almost of three orders of magnitude. Conversely, the discrepancies between the reference results derived in Sec. III C and the ones assuming a partial or a complete hydrogenlike model are rather small. The main difference between diagrams 2 and 3 lies in the number of states concerned. In the case of diagram 3, the number of states is considerably increased (by a factor of  $10^8$  in order of magnitude). We see that this very important increase does not change the value of the global ionization rate. As a result, the value of the global rate coefficient mainly depends on the distribution of levels between the ground state and the ionization limit, regardless of the statistical weights, therefore of the number of states. The energy diagrams of carbon, nitrogen, and oxygen are similar. The rate coefficients derived in our approach are then very close to each other for these three species.

### E. Global rate coefficients and equilibrium constant

$k_i$  and  $k_r$  values are often correlated to the Saha equilibrium constant  $K^S$  according to Eq. (28).<sup>32,120</sup> We have previously indicated that this is not correct owing to the behavior of the excited states. We can illustrate this fundamental aspect by calculating the ratio  $\frac{k_i}{k_r K^S}$ . The results are displayed on Fig. 9. If  $T_e < 15\,000$  K, the ratio is close to unity, which means that  $k_i/k_r$  is close to  $K^S$ . Conversely, a difference appears around 15 000 K, the value of which increases with  $T_e$ . The higher the temperature  $T_e$ , the higher  $k_i/k_r$  is in comparison with  $K^S$ . We can notice that two groups of species seem to constitute. The first group includes nitrogen and oxygen which present a similar behavior for  $\frac{k_i}{k_r K^S}$  relatively close to unity with a discrepancy less than 10% for  $T_e < 20\,000$  K. The second group includes carbon and argon with larger discrepancies reaching 20% at 20 000 K. The accurate determination of  $k_i$  and  $k_r$  is sometimes difficult for C so that the ratio  $\frac{k_i}{k_r K^S}$  departs from unity at low temperature. This difficulty results from the behavior of the metastable states. The significant difference between C and the other species lies in the number of metastable states and their excitation energy.

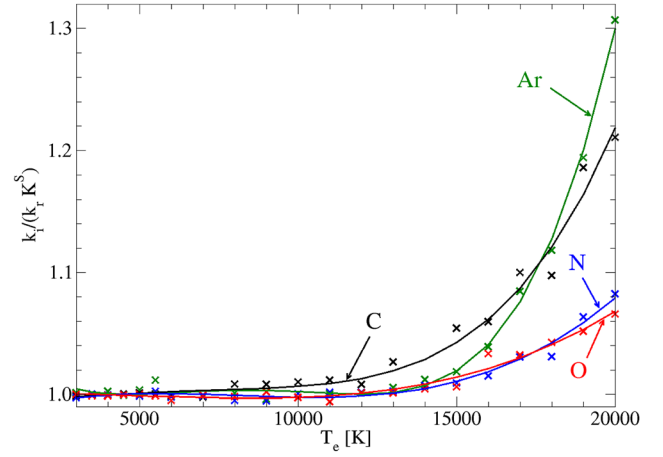


FIG. 9. Ratio  $\frac{k_i}{k_r K^S}$  versus temperature  $T_e$ . The crosses (carbon-black, nitrogen-blue, oxygen-red, and argon-green) correspond to the results and the lines to trends given by interpolations using polynomials of the third order over the range  $3000\text{ K} \leq T_e \leq 20\,000\text{ K}$ . The ratio increases with  $T_e$ . This indicates that a global rate coefficient ( $k_i$  or  $k_r$ ) can be derived from the complementary rate coefficient ( $k_r$  or  $k_i$ , respectively) using the Saha equilibrium law at low temperature only.

The five metastable states of C correspond to an intermediate energy, between 0.002 eV and 4.18 eV. Starting from a nonequilibrium configuration, one observes first a progressive coupling between the excited states and a part of the metastable states, especially state  $^5S_2^o$ . During this phase, the evolution of the other metastable states is small. Afterwards, their evolution is amplified until equilibrium is reached. The QSS is therefore not at all obvious and leads to an inaccurate estimate of the global rate coefficient. We estimated that the ratio  $\frac{k_i}{k_r K^S}$  is then reliable at  $\pm 5\%$  for C. As a result, the discrepancy between  $k_i/k_r$  and  $K^S$  is significant only for  $T_e > 17\,000$  K as shown by Fig. 9.

Conversely, for the other species, the determination can be performed with a satisfactory precision. As a result, the ratio  $\frac{k_i}{k_r K^S}$  presents a small dispersion around the mean evolution, and the increase with  $T_e$  is then significant for the entire range 3000 K–20 000 K. In order to confirm the trend  $\frac{d}{dT_e} \left( \frac{k_i}{k_r K^S} \right) > 0$  for argon the dynamics of which is the strongest one, we have performed the calculation of  $k_i$  and  $k_r$  at higher temperatures. The resulting values for  $\frac{k_i}{k_r K^S}$  are approximately equal to 10 at 35 000 K, and to 100 at 50 000 K. The ratio  $k_i/k_r$  increases more strongly with  $T_e$  than the equilibrium constant  $K^S$ . Generally speaking, ratio  $k_i/k_r$  therefore departs from  $K^S$ . The interpretation of this departure has to be studied more specifically, notably by extending the theoretical framework of our approach. For example, we have to account for the ionization potential lowering due to the Debye shielding resulting from high electron densities encountered at high temperature. This study is postponed for future work.

Nevertheless, the influence of the excited states can be discussed. The level of population density of these excited states during the quasi-steady state depends on pressure  $p$ , temperature  $T_e$ , and the initial conditions of  $n_e$  and  $T_{exc}$ . When  $n_e$  or  $T_{exc}$  is changed, the densities of excited states are different during the quasi-steady state. Nevertheless,  $p$  and  $T_e$  remaining unchanged, the rate coefficient (obtained



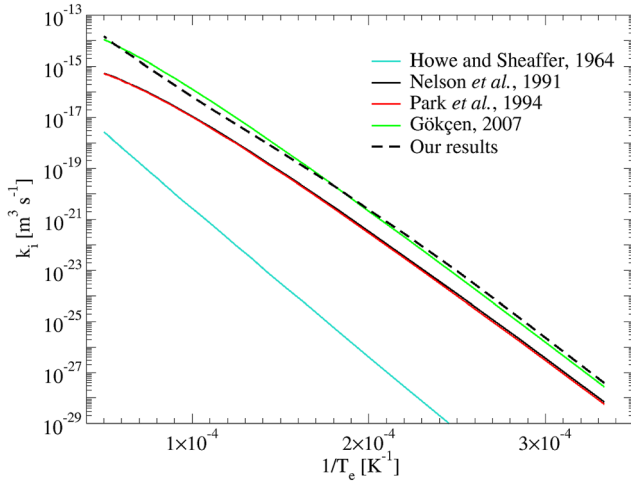


FIG. 10. Comparison between the carbon global ionization rate coefficients  $k_i$  obtained in this study and existing data.

by identification with  $k_{i,r}^*$  during the QSS) also remains unchanged. As a result, the discrepancy between  $k_i/k_r$  and the Saha equilibrium constant  $K^S$  is the same. The values obtained for the population densities have therefore no influence on this discrepancy.

## F. Global rate coefficients compared with other existing data

In the literature, many data are available concerning either  $k_i$  or  $k_r$  for carbon, nitrogen, oxygen, and argon so that an exhaustive comparison cannot be performed. Of course, we have systematically rejected the rate coefficients resulting from integration according to Eq. (8) of cross sections corresponding to the direct ionization from the atomic ground state to the ionic ground state and conversely for the recombination. Indeed, these rate coefficients [equal to (34) for ionization] do not describe the ionization or the recombination of the mixture due to the coupling between all the excited and ground states resulting from the elementary processes of Secs. II B and II C, and illustrated by Fig. 1. This leads to a drastic reduction of rate coefficients, the

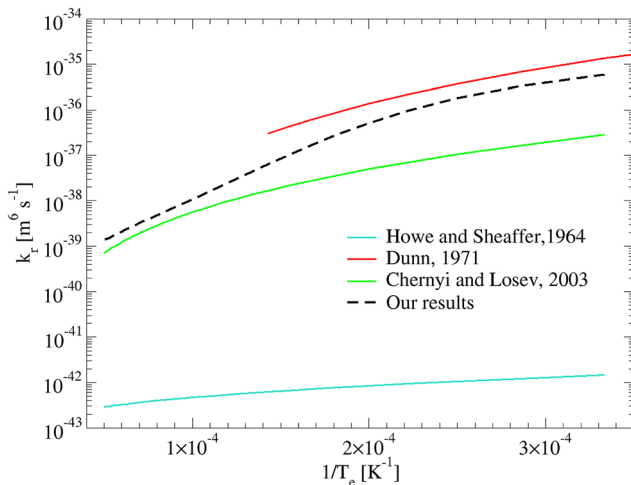


FIG. 11. Comparison between the  $C^+$  global recombination rate coefficients  $k_r$  obtained in this study and existing data.

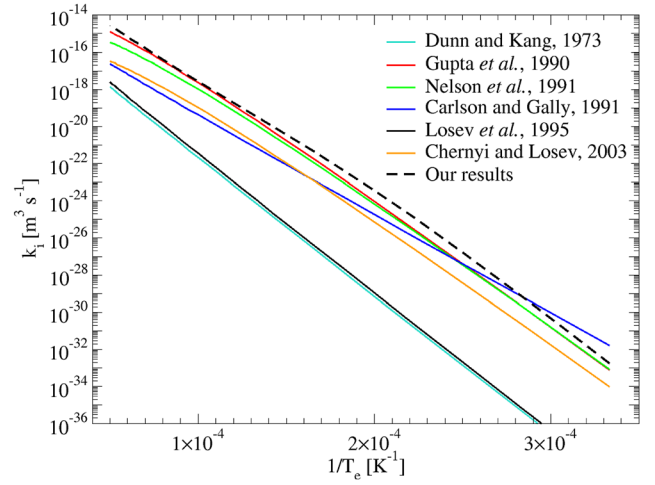


FIG. 12. Comparison between the nitrogen global ionization rate coefficients  $k_i$  obtained in this study and existing data.

values of which can be compared with our results. Moreover, the most widely used data generally presented under analytic forms have been preferred. The hypothesis of Eq. (28) is usually assumed by the different authors, so that we have used their equilibrium constant  $K^S$  when the value is given in order to derive the rate coefficient for the complementary process. The possible discrepancy between results at high temperature must be therefore considered cautiously.

## 1. Carbon

Among the species studied in this paper, carbon is the one for which the data are the rarest. Figure 10 displays these data for the ionization<sup>38,47,121,122</sup> compared with ours, and Fig. 11 the ones related to the recombination.<sup>121,123,124</sup> Except the results of Howe and Shaeffer<sup>121</sup> which are far from the others, the rate coefficients are relatively close. The ionization rate is in good agreement with the one due to Gökçen.<sup>122</sup> For the recombination, our results make the continuity between the results of Dunn<sup>123</sup> at low temperature, which have been obtained experimentally, and those of Chernyi and Losev<sup>124</sup> at high temperature.

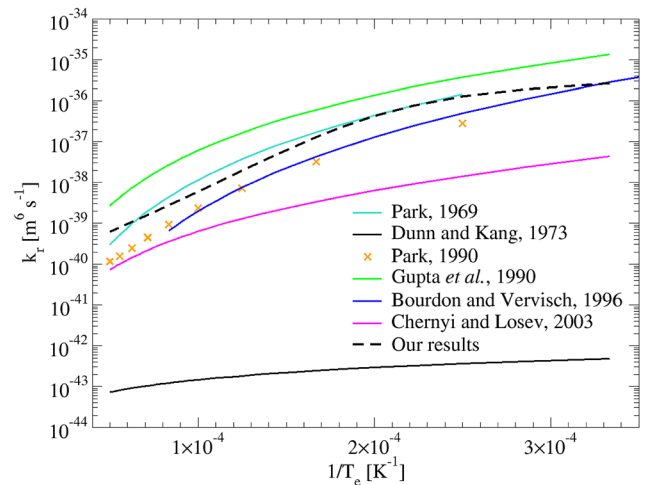


FIG. 13. Comparison between the  $N^+$  global recombination rate coefficients  $k_r$  obtained in this study and existing data.



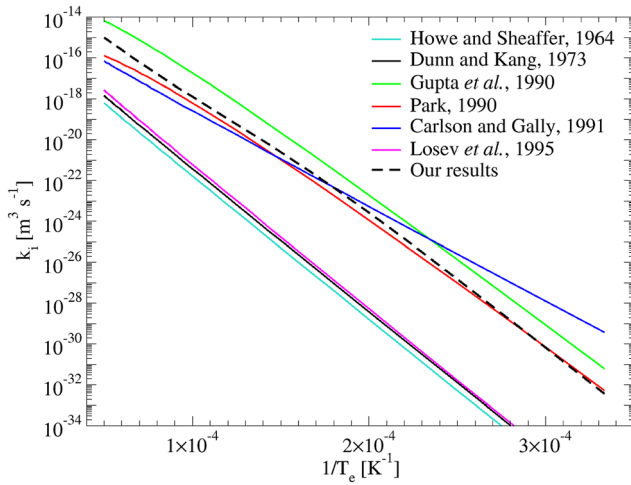


FIG. 14. Comparison between the oxygen global ionization rate coefficients  $k_i$  obtained in this study and existing data.

## 2. Nitrogen

Our ionization rates are compared with reference data<sup>38,124–128</sup> on Fig. 12. Our recombination rates are compared with literature data<sup>66,124–126,129</sup> on Fig. 13. We can notice that our results correspond to high values within the range given by literature. In particular, for the ionization, our results agree well with the ones of Gupta *et al.*<sup>126</sup> at high temperature and with the ones of Carlson and Gally<sup>127</sup> at low temperature. For the recombination, the agreement with the data of Bourdon and Vervisch<sup>66</sup> is pretty good at low temperature whereas the agreement is obtained at high temperature with the data of Park.<sup>129</sup> It is interesting to note that the recombination rates due to Park have been obtained experimentally<sup>130</sup> and confirmed theoretically by Park using another cross sections set than the one due to Drawin.

## 3. Oxygen

Figure 14 illustrates the comparison between our results and reference data<sup>32,121,125–128</sup> for ionization. Our results are close to those due to Park once again, but related to more recent work.<sup>32</sup> Our results are also close to the data of

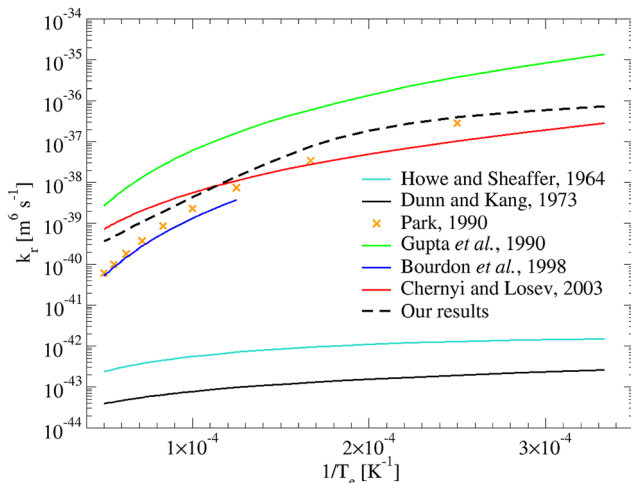


FIG. 15. Comparison between the  $O^+$  global recombination rate coefficients  $k_r$  obtained in this study and existing data.

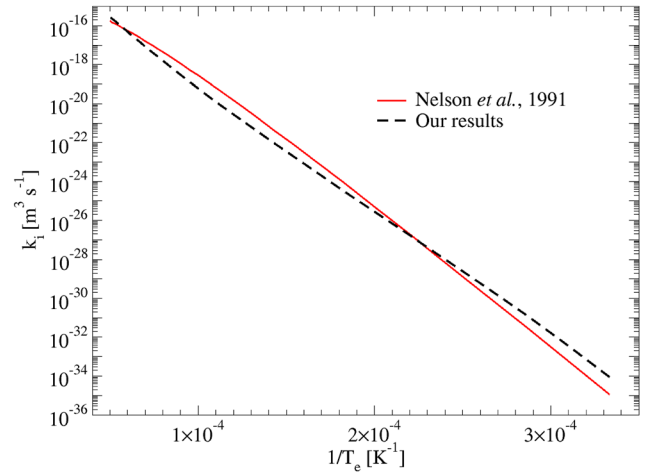


FIG. 16. Comparison between the argon global ionization rate coefficients  $k_i$  obtained in this study and existing data.

Carlson and Gally.<sup>127</sup> Figure 15 illustrates the same comparison, but for recombination.<sup>32,67,121,124–126</sup> In this case, the results of Chernyi and Losev<sup>124</sup> are close to ours at high temperature whereas the agreement is better with the ones of Park<sup>32</sup> at low temperature.

## 4. Argon

The evolution with  $T_e$  of the ionization rate coefficient due to Nelson *et al.*<sup>38</sup> is displayed on Fig. 16. In the paper of Nelson *et al.*, the ionization rate coefficient is given for N, C, H, and Ar. Neither the nature of the collision partner nor the source from which data are derived is indicated in this paper. For N, the rate is the same as the one due to Park<sup>32</sup> where the collision partner is an electron. We have therefore assumed that the ionization rate coefficient for argon given by Nelson *et al.* is related to electron-induced processes. We can notice an excellent agreement with our results.

For the recombination, different rate coefficients<sup>69,114,131–133</sup> are displayed on Fig. 17. The results of Bates *et al.*<sup>131</sup> have been obtained with a cross sections set due to Gryzinski,<sup>74</sup> which has been in part used by Bourdon

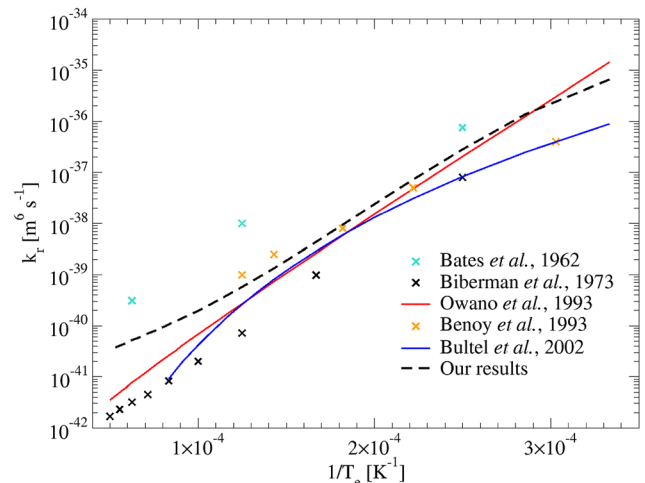


FIG. 17. Comparison between the  $Ar^+$  global recombination rate coefficients  $k_r$  obtained in this study and existing data.

*et al.*<sup>66,67</sup> for the study of nitrogen and oxygen recombinations. The rates obtained by Bates *et al.* are higher than the ones obtained in the present paper. Moreover, the rates obtained by Bourdon *et al.* for N and O are lower than what we have calculated. Our results finally succeed in reproducing a satisfactory mean behavior.

The recombination rates obtained by us in 2002 (Ref. 69) are based on an energy diagram resulting from the lump of states in fictitious levels according to Vlček.<sup>7</sup> We put forward in Sec. III D the influence of this procedure on the global rate coefficient. The rate is underestimated. As a result, the rate coefficients are higher as illustrated by Fig. 17 and reach the results of Owano *et al.*<sup>133</sup> at low temperature, and of Benoy *et al.*<sup>114</sup> at high temperature. The recombination rates obtained for Ar are therefore in relatively good agreement with other recent data.

#### IV. CONCLUSION

In this paper, we have investigated the dynamics of the excited and ground states of carbon, nitrogen, oxygen, and argon and their parent ion in nonequilibrium conditions and derived the global rate coefficients for ionization and recombination over the range  $3000 \text{ K} \leq T_e \leq 20\,000 \text{ K}$  using the same cross sections set. This set, due to Drawin,<sup>89</sup> takes into account the electric dipolar allowed and forbidden transitions. These global rate coefficients have been determined after the correct identification of the conditions during which the concept of global rate coefficient is relevant. Global rate coefficients are defined during a quasi-steady state. The influence of the excited states distribution and the underlying dynamics due to the elementary processes has been studied. The results have shown that the discretization in energy has to be sufficiently refined to avoid any underestimate of the global rate coefficients. Since the global rate coefficients of ionization  $k_i$  and recombination  $k_r$  are determined using a state-to-state approach, the departure of their ratio from the Saha equilibrium constant can be calculated. The results show a negligible departure for temperature less than  $15\,000 \text{ K}$  for the species considered. For higher temperatures, the departure can reach 20% at  $20\,000 \text{ K}$  (case of argon). Some preliminary calculations performed at  $35\,000 \text{ K}$  and  $50\,000 \text{ K}$  seem to show that this departure tends to increase with temperature. The previous levels of temperature exceeding the validity range of our approach, these results have to be confirmed within the framework of additional works. The comparison of the results obtained in the present study with former results exhibits a pretty good agreement, notably concerning recent data. Finally, the rate coefficients have been systematically interpolated under a modified Arrhenius law. They will be used in plasma flows CFD calculations. Despite this general good agreement, we are performing the same type of calculations with the cross sections obtained in part with the HULLAC package.<sup>134</sup> We will then estimate the influence of a quantum approach of the elementary processes on the rate coefficients.

The present work has three important perspectives. First, we will implement the global rate coefficients  $k_i$  and  $k_r$  in computational fluid dynamics codes for high enthalpy

$\text{CO}_2\text{-N}_2\text{-Ar}$  flows for Martian entries. Behind a strong shock wave, the quick dissociation of  $\text{CO}_2$  and  $\text{N}_2$  in CO, C, O, and N leads to the formation of atoms whose associative ionization (for example,<sup>135</sup>  $\text{N} + \text{O} \rightarrow \text{NO}^+ + e^-$ ) creates the first electrons. When the dissociation degree is sufficiently high, the previous processes are replaced in terms of frequency and efficiency by direct ionization through electron-induced processes. Testing these new global rate coefficients and analyzing the results will be particularly valuable. Within this context, the properties of the downstream flow far from the shock front will be discussed in the light of the discrepancy between the ratio  $k_i/k_r$  and the Saha equilibrium constant.

The second important perspective is to study further this departure of  $k_i/k_r$  from the Saha equilibrium constant, by extending at higher temperature levels the framework of the present calculations. The fact that the excited states are overpopulated in case of recombination or underpopulated in case of ionization induces that  $k_i$  and  $k_r$  cannot be used simultaneously. In this context, how to obtain with global rate coefficients the composition of a mixture when equilibrium is reached? The problem of the determination of an equilibrium composition using global rate coefficients is therefore totally open and is crucial in CFD calculations.

The procedure developed in the present paper can also be adapted to any global kinetic mechanism, the dynamics of which depends on stepwise elementary processes. The third expected perspective consists in determining the rate coefficient for dissociation and recombination of molecules by excitation-deexcitation of the vibrational modes under heavy particles impact taking into account mono and multi-quanta jumps. We are currently analyzing the dissociation of  $\text{CO}_2$  from this point of view.<sup>136</sup>

#### ACKNOWLEDGMENTS

We wish to acknowledge the French Spatial Agency CNES, the French ANR Project *RAYHEN*, and the European project *Phys4Entry* (Seventh Framework Program) for their scientific and financial support.

- <sup>1</sup>B. Evans, K. Morgan, and O. Hassan, *Appl. Math. Model.* **35**, 996 (2011).
- <sup>2</sup>M. C. Bordage, P. Ségur, L. G. Christophorou, and J. K. Olthoff, *J. Appl. Phys.* **86**, 3558 (1999).
- <sup>3</sup>A. Gleizes, J. J. Gonzalez, and P. Freton, *J. Phys. D: Appl. Phys.* **38**, R153 (2005).
- <sup>4</sup>P. D. Feldman, *Astron. Astrophys.* **70**, 547 (1978).
- <sup>5</sup>G. Gousset, M. Touzeau, M. Vialle, and C. M. Ferreira, *Plasma Chem. Plasma Process.* **9**, 189 (1989).
- <sup>6</sup>J. J. Lowke and R. Morrow, *Pure Appl. Chem.* **66**, 1287 (1994).
- <sup>7</sup>J. Vlček, *J. Phys. D: Appl. Phys.* **22**, 623 (1989).
- <sup>8</sup>K. P. Singh and S. Roy, *J. Appl. Phys.* **101**, 123308 (2007).
- <sup>9</sup>M. Capitelli, A. Casavola, G. Colonna, and A. D. Giacomo, *Spectrochim. Acta B* **59**, 271 (2004).
- <sup>10</sup>G. Colonna, A. Casavola, and M. Capitelli, *Spectrochim. Acta B* **56**, 567 (2001).
- <sup>11</sup>H. C. Le, D. E. Zeitoun, J. D. Parisse, M. Sentis, and W. Marine, *Phys. Rev. E* **62**, 4152 (2000).
- <sup>12</sup>N. Atsuchi, M. Shigeta, and T. Watanabe, *Int. J. Heat Mass Transfer* **49**, 1073 (2006).
- <sup>13</sup>K. T. A. L. Burm, B. Jodoin, P. Proulx, and M. I. Boulos, *Plasma Sources Sci. Technol.* **12**, 362 (2003).
- <sup>14</sup>M. Panesi, P. Rini, G. Degrez, and O. Chazot, *J. Thermophys. Heat Transfer* **21**, 57 (2007).

- <sup>15</sup>K. Takechi and M. A. Lieberman, *J. Appl. Phys.* **90**, 3205 (2001).
- <sup>16</sup>Y. Tanaka and T. Sakuta, *J. Phys. D: Appl. Phys.* **35**, 468 (2002).
- <sup>17</sup>C. H. Chang and E. Pfender, *Plasma Chem. Plasma Process.* **10**, 473 (1990).
- <sup>18</sup>C. H. Chang and J. D. Ramshaw, *Plasma Chem. Plasma Process.* **16**, 5S (1996).
- <sup>19</sup>T. W. Megli, H. Krier, and R. L. Burton, *J. Thermophys. Heat Transfer* **10**, 554 (1996).
- <sup>20</sup>K. S. C. Peerenboom, W. J. Goodheer, J. van Dijk, and J. J. A. M. van der Mullen, *Plasma Sources Sci. Technol.* **19**, 025009 (2010).
- <sup>21</sup>G. E. Georgiou, A. P. Papadakis, R. Morrow, and A. Metaxas, *J. Phys. D: Appl. Phys.* **38**, R303 (2005).
- <sup>22</sup>A. B. Murphy and T. McAllister, *Phys. Plasmas* **8**, 2565 (2001).
- <sup>23</sup>R. Ye, A. B. Murphy, and T. Ishigaki, *Plasma Chem. Plasma Process.* **27**, 189 (2007).
- <sup>24</sup>Y. Tanaka, T. Michishita, and Y. Uesugi, *Plasma Sources Sci. Technol.* **14**, 134 (2005).
- <sup>25</sup>J.-B. Belhaouari, J.-J. Gonzalez, and A. Gleizes, *J. Phys. D: Appl. Phys.* **31**, 1219 (1998).
- <sup>26</sup>A. Kaminska, B. Lopez, B. Izrar, and M. Dudeck, *Plasma Sources Sci. Technol.* **17**, 035018 (2008).
- <sup>27</sup>J. Park, J. Heberlein, E. Pfender, G. Candler, and C. H. Chang, *Plasma Chem. Plasma Process.* **28**, 213 (2008).
- <sup>28</sup>M. S. Benilov, B. V. Rogov, A. I. Sokolova, and G. A. Tirsikii, *J. Appl. Mech. Tech. Phys.* **27**, 653 (1986).
- <sup>29</sup>S. V. Zhukotov and T. Abe, *J. Thermophys. Heat Transfer* **13**, 50 (1999).
- <sup>30</sup>S. Ghorui, J. V. R. Heberlein, and E. Pfender, *J. Phys. D: Appl. Phys.* **40**, 1966 (2007).
- <sup>31</sup>H.-M. Damevin and K. A. Hoffmann, *J. Thermophys. Heat Transfer* **16**, 498 (2002).
- <sup>32</sup>C. Park, *Nonequilibrium Hypersonic Aerothermodynamics* (John Wiley & Sons, New York, 1990).
- <sup>33</sup>J. M. Reese, M. A. Gallis, and D. A. Lockerby, *Philos. Trans. R. Soc. London A* **361**, 2967 (2003).
- <sup>34</sup>E. Buccignani and G. Pezzella, *Math. Comput. Simul.* **81**, 656 (2010).
- <sup>35</sup>T. A. Gally, L. A. Carlson, and D. Green, *J. Thermophys. Heat Transfer* **7**, 285 (1993).
- <sup>36</sup>R. N. Gupta, J. N. Moss, and J. M. Price, *J. Thermophys. Heat Transfer* **11**, 562 (1997).
- <sup>37</sup>J. Lee, A. Orsini, and S. M. Ruffin, *J. Thermophys. Heat Transfer* **24**, 18 (2010).
- <sup>38</sup>H. F. Nelson, C. Park, and E. E. Whiting, *J. Thermophys.* **5**, 157 (1991).
- <sup>39</sup>D. R. Olynick, W. D. Henline, L. H. Chambers, and G. V. Candler, *J. Thermophys. Heat Transfer* **9**, 586 (1995).
- <sup>40</sup>T. Ozawa, T. Suzuki, H. Takayanagi, and K. Fujita, *J. Thermophys. Heat Transfer* **25**, 341 (2011).
- <sup>41</sup>C. Park and S. Yoon, *AIAA J.* **30**, 999 (1992).
- <sup>42</sup>G. Tchen and D. E. Zeitoun, *Int. J. Heat Fluid Flow* **29**, 1393 (2008).
- <sup>43</sup>R. W. Walters, P. Cinnella, D. C. Slack, and D. Halt, *AIAA J.* **30**, 1304 (1992).
- <sup>44</sup>C. Rond, P. Boubert, J.-M. Félio, and A. Chikhaoui, *Chem. Phys.* **340**, 93 (2007).
- <sup>45</sup>D. R. Mott, T. A. Gally, and L. A. Carlson, *J. Thermophys. Heat Transfer* **9**, 577 (1995).
- <sup>46</sup>C. Park, *J. Thermophys. Heat Transfer* **7**, 385 (1993).
- <sup>47</sup>C. Park, J. T. Howe, R. L. Jaffe, and G. V. Candler, *J. Thermophys. Heat Transfer* **8**, 9 (1994).
- <sup>48</sup>G. Degrez, A. Lani, M. Panesi, O. Chazot, and H. Deconinck, *J. Phys. D: Appl. Phys.* **42**, 194004 (2009).
- <sup>49</sup>D. Zeitoun, E. Boccaccio, M.-C. Druguet, and M. Imbert, *AIAA J.* **32**, 333 (1994).
- <sup>50</sup>M. Capitelli, I. Armenise, D. Bruno, M. Cacciatore, R. Celiberto, G. Colonna, O. D. Pascale, P. Diomedede, F. Esposito, G. Gorse, K. Hassouni, A. Laricchiuta, S. Longo, D. Pagano, D. Pietanza, and M. Rutigliano, *Plasma Sources Sci. Technol.* **16**, 830 (2007).
- <sup>51</sup>M. Capitelli, R. Celiberto, G. Colonna, G. D'Ammando, O. D. Pascale, P. Diomedede, F. Esposito, G. Gorse, A. Laricchiuta, S. Longo, L. D. Pietanza, and F. Taccogna, *Plasma Phys. Controlled Fusion* **53**, 124007 (2011).
- <sup>52</sup>A. Prakash, N. Parsons, X. Wang, and X. Zhong, *J. Comput. Phys.* **230**, 8474 (2011).
- <sup>53</sup>F. Coquel, C. Flament, V. Joly, and C. Marmignon, "Viscous nonequilibrium flow cancellations," in *Computing Hypersonic Flows* (Birkhauser, Boston, 1993).
- <sup>54</sup>A. Lani, Ph.D. dissertation, von Karman Institute, 2008.
- <sup>55</sup>M. J. Wright, G. V. Candler, and D. Bose, *AIAA J.* **36**, 1603 (1998).
- <sup>56</sup>P. A. Gnoffo, R. N. Gupta, and J. L. Shinn, "Conservation equations and physical models for hypersonic air flows in thermal and chemical non-equilibrium," Technical Report No. TP-2867, NASA, 1989.
- <sup>57</sup>L. M. G. Walpot, G. Simeonides, J. Muylaert, and P. G. Bakker, *Shock Waves* **6**, 197 (1996).
- <sup>58</sup>S. T. Surzhikov, *Fluid Dyn.* **46**, 490 (2011).
- <sup>59</sup>M. Netterfield, "Proceedings of the 27th thermophysics conference," AIAA Paper No. 92-2878, 1992.
- <sup>60</sup>O. Knab, H.-H. Frühauf, and E. W. Messerschmid, in *Proceedings of the Second European Symposium Aerothermodynamics for Space Vehicles* (ESA Publications Division, 1995), Vol. 129.
- <sup>61</sup>I. Nompelis, T. W. Drayna, and G. V. Candler, "Proceedings of the 34th fluid dynamics conference," AIAA Paper No. 2004-2227, 2004.
- <sup>62</sup>R. H. Bush, G. D. Powder, and C. E. Towne, "Proceedings of the 36th aerospace sciences meeting and exhibit," AIAA Paper no. 98-0935, 1998.
- <sup>63</sup>G. Colonna, I. Armenise, D. Bruno, and M. Capitelli, *J. Thermophys. Heat Transfer* **20**, 477 (2006).
- <sup>64</sup>W. H. Soon and J. A. Kunc, *Phys. Rev. A* **41**, 825 (1990).
- <sup>65</sup>J. A. Kunc and W. H. Soon, *Phys. Rev. A* **40**, 5822 (1989).
- <sup>66</sup>A. Bourdon and P. Vervisch, *Phys. Rev. E* **54**, 1888 (1996).
- <sup>67</sup>A. Bourdon, Y. Teresiak, and P. Vervisch, *Phys. Rev. E* **57**, 4684 (1998).
- <sup>68</sup>K. Sawada and T. Fujimoto, *Phys. Rev. E* **49**, 5565 (1994).
- <sup>69</sup>A. Bultel, B. van Ootegem, A. Bourdon, and P. Vervisch, *Phys. Rev. E* **65**, 046406 (2002).
- <sup>70</sup>See <http://www.nist.gov/pml/data/asd.cfm> for NIST.
- <sup>71</sup>H. R. Griem, *Plasma Spectroscopy* (McGraw-Hill, New York, 1964).
- <sup>72</sup>W. Ebeling and I. Leike, *Physica A* **170**, 682 (1991).
- <sup>73</sup>T. Bornath, M. Schlages, F. Morales, and R. Prenzler, *J. Quant. Spectrosc. Radiat. Transf.* **58**, 501 (1997).
- <sup>74</sup>M. Gryzinski, *Phys. Rev.* **115**, 374 (1959).
- <sup>75</sup>A. E. Kingston, *Phys. Rev.* **135**, A1537 (1964).
- <sup>76</sup>H. van Regemorter, *Astrophys. J.* **136**, 906 (1962).
- <sup>77</sup>L. A. Vainshtein, *Opt. Spectrosc.* **18**, 538 (1965).
- <sup>78</sup>P. L. Bartlett and A. T. Stelbovics, *Phys. Rev. A* **66**, 012707 (2002).
- <sup>79</sup>M. Inokuti, *Rev. Mod. Phys.* **43**, 297 (1971).
- <sup>80</sup>Y.-K. Kim and M. E. Rudd, *Phys. Rev. A* **50**, 3954 (1994).
- <sup>81</sup>K. Bartschat and D. H. Madison, *J. Phys. B: At. Mol. Phys.* **20**, 5839 (1987).
- <sup>82</sup>J. Gao, D. H. Madison, and J. L. Peachner, *J. Chem. Phys.* **123**, 204314 (2005).
- <sup>83</sup>K. Bartschat and P. G. Burke, *J. Phys. B: At. Mol. Phys.* **20**, 3191 (1987).
- <sup>84</sup>I. Kanik, P. V. Johnson, M. B. Das, M. A. Khakoo, and S. S. Tayal, *J. Phys. B: At. Mol. Opt. Phys.* **34**, 2647 (2001).
- <sup>85</sup>M. S. Pindzola and F. J. Robicheaux, *Phys. Rev. A* **61**, 052707 (2000).
- <sup>86</sup>I. Bray and A. T. Stelbovics, *Adv. At. Mol. Phys.* **35**, 209 (1995).
- <sup>87</sup>M. Baertschy, T. N. Rescigno, W. A. Isaacs, X. Li, and C. W. McCurdy, *Phys. Rev. A* **63**, 022712 (2001).
- <sup>88</sup>A. Bar-Shalom, M. Klapisch, and J. Oreg, *J. Quant. Spectrosc. Radiat. Transf.* **71**, 169 (2001).
- <sup>89</sup>H. W. Drawin, in *Collision and Transport Cross-Sections*, EUR-CEA-FC 383 (Association EURATOM-CEA, Département de recherches sur la fusion contrôlée, 1966).
- <sup>90</sup>W. Lotz, *Z. Phys.* **216**, 241 (1968).
- <sup>91</sup>L. Vriens and A. H. M. Smeets, *Phys. Rev. A* **22**, 940 (1980).
- <sup>92</sup>V. A. Bernshtam, Y. V. Ralchenko, and Y. Maron, *J. Phys. B: At. Mol. Opt. Phys.* **33**, 5025 (2000).
- <sup>93</sup>Y.-K. Kim, *Phys. Rev. A* **64**, 032713 (2001).
- <sup>94</sup>M. Kapper and J.-L. Cambier, *J. Appl. Phys.* **109**, 113308 (2011).
- <sup>95</sup>M. Kapper and J.-L. Cambier, *J. Appl. Phys.* **109**, 113309 (2011).
- <sup>96</sup>M. Panesi, T. E. Magin, A. Bourdon, A. Bultel, and O. Chazot, *J. Thermophys. Heat Transfer* **25**, 361 (2011).
- <sup>97</sup>A. Bultel, B. G. Chéron, A. Bourdon, O. Motapon, and I. F. Schneider, *Phys. Plasmas* **13**, 043502 (2006).
- <sup>98</sup>A. Gomes, A. Essoltani, and J. Bacri, *J. Quant. Spectrosc. Radiat. Transf.* **43**, 471 (1990).
- <sup>99</sup>A. Hartgers, J. van Dijk, J. Jonkers, and J. A. M. van der Mullen, *Comput. Phys. Commun.* **135**, 199 (2001).
- <sup>100</sup>C. O. Laux, L. Pierrot, and R. J. Gessman, *Chem. Phys.* **398**, 46-55 (2012).
- <sup>101</sup>J.-P. Sarrette, A. M. Gomes, J. Bacri, C. O. Laux, and C. H. Kruger, *J. Quant. Spectrosc. Radiat. Transf.* **53**, 125 (1995).

- <sup>102</sup>Y. E. E. Gamal, M. A. Mahmoud, and H. A. A. El-Rahman, *J. Quant. Spectrosc. Radiat. Transf.* **90**, 29 (2005).
- <sup>103</sup>V. Morel, A. Bultel, and B. G. Chéron, *Spectrochim. Acta B* **65**, 830 (2010).
- <sup>104</sup>A. Yanguas-Gil, J. Cotrino, and L. L. Alves, *J. Phys. D: Appl. Phys.* **38**, 1588 (2005).
- <sup>105</sup>S. Roy and B. P. Pandey, *Phys. Plasmas* **9**, 4052 (2002).
- <sup>106</sup>V. Morel, Ph.D. dissertation, Université de Rouen, 2011.
- <sup>107</sup>A. J. MacLeod, *J. Comput. Appl. Math.* **148**, 363 (2002).
- <sup>108</sup>H. Nussbaumer and P. J. Storey, *Astron. Astrophys.* **126**, 75 (1983).
- <sup>109</sup>H. Nussbaumer and P. J. Storey, *Astron. Astrophys. Suppl. Ser.* **56**, 293 (1984).
- <sup>110</sup>M. S. Peters and E. J. Skorpinski, *J. Chem. Educ.* **42**, 329 (1965).
- <sup>111</sup>R. D. Taylor and A. W. Ali, *J. Quant. Spectrosc. Radiat. Transf.* **35**, 213 (1986).
- <sup>112</sup>J. W. Bond, K. M. Watson, and J. A. Welch, *Atomic Theory of Gas Dynamics* (Addison-Wesley Publishing Company, Inc., Massachusetts, 1965).
- <sup>113</sup>M. I. Hoffert and H. Lien, *Phys. Fluids* **10**, 1769 (1967).
- <sup>114</sup>D. A. Benoy, J. A. M. van der Mullen, M. C. M. van de Sanden, B. van der Sijde, and D. C. Schram, *J. Quant. Spectrosc. Radiat. Transf.* **49**, 129 (1993).
- <sup>115</sup>C. H. Chang and J. D. Ramshaw, *Phys. Plasmas* **1**, 3698 (1994).
- <sup>116</sup>S. P. Fusselman and H. K. Yasuda, *Plasma Chem. Plasma Process.* **14**, 251 (1994).
- <sup>117</sup>S. E. Selezneva, V. Sember, D. V. Gravelle, and M. I. Boulos, *J. Phys. D: Appl. Phys.* **35**, 1338 (2002).
- <sup>118</sup>I. Shimamura and T. Fujimoto, *Phys. Rev. A* **42**, 2346 (1990).
- <sup>119</sup>M. Abramowitz and I. Stegun, *Handbook of Mathematical Functions* (Dover, New York, 1965).
- <sup>120</sup>G. George, G. Candler, and E. Pfender, *J. Phys. D: Appl. Phys.* **31**, 2269 (1998).
- <sup>121</sup>J. T. Howe and Y. S. Shaeffer, "Chemical relaxation behind strong normal shock waves in carbon dioxide including interdependent dissociation and ionization processes," NASA TN D-2131, 1964, (unpublished).
- <sup>122</sup>T. Gökçen, *J. Thermophys. Heat Transfer* **21**, 9 (2007).
- <sup>123</sup>M. G. Dunn, *AIAA J.* **9**, 2184 (1971).
- <sup>124</sup>G. G. Chernyi and S. A. Losev, "Problems of aerothermodynamics, radiation gasdynamics, heat and mass transfer for planet sample return missions," ISTC 1549-00, 2003, (unpublished).
- <sup>125</sup>M. G. Dunn and S. W. Kang, "Theoretical and experimental studies of reentry plasmas," NASA CR 2232, 1973, (unpublished).
- <sup>126</sup>R. N. Gupta, J. M. Yos, R. A. Thompson, and K. P. Lee, "A review of reaction rates and thermodynamic and transport properties for an 11 species air model for chemical and thermal nonequilibrium calculations to 30000 K," NASA RP 1232, 1990, (unpublished).
- <sup>127</sup>L. A. Carlson and T. A. Gally, *J. Thermophys.* **5**, 9 (1991).
- <sup>128</sup>S. A. Losev, V. N. Makarov, and M. Y. Pogosbekyan, *Fluid Dyn.* **30**, 299 (1995).
- <sup>129</sup>C. Park, *AIAA J.* **7**, 1653 (1969).
- <sup>130</sup>C. Park, *AIAA J.* **6**, 2090 (1968).
- <sup>131</sup>D. R. Bates, A. E. Kingston, and R. W. P. McWhirter, *Proc. R. Soc. London, Ser. A* **267**, 297 (1962).
- <sup>132</sup>L. M. Biberman, V. S. Vorob'ev, and Y. T. Yakubov, *Sov. Phys. Usp.* **15**, 375 (1973).
- <sup>133</sup>T. G. Owano, C. H. Kruger, and R. A. Beddini, *AIAA J.* **31**, 75 (1993).
- <sup>134</sup>J. Kuba, R. F. Smith, D. Benredjem, C. Möller, L. Upcraft, R. King, A. Klisnick, L. Drska, G. J. Pert, and J.-C. Gauthier, *J. Opt. Soc. Am. B* **20**, 208 (2003).
- <sup>135</sup>O. Motapon, M. Fidirig, A. Florescu, F.-O. Waffeu-Tamo, O. Crumeyrolle, G. Varin-Bréant, A. Bultel, P. Vervisch, J. Tennyson, and I. F. Schneider, *Plasma Sources Sci. Technol.* **15**, 23 (2006).
- <sup>136</sup>J. Annaloro, A. Bultel, and P. Omaly, "Proceedings of the 42nd thermo-physics conference," AIAA Paper No. 2011-3954, 2011.